Time scale of diffusion in molecular and cellular biology

2014 J. Phys. A: Math. Theor. 47 173001

IOP Publishing Journal of Physics A: Mathematical and Theoretical
J. Phys. A: Math. Theor. **47** (2014) 173001 (50pp) doi:10.1088/1751-8113/47/17/173001

Topical Review

Time scale of diffusion in molecular and cellular biology

D Holcman[1] **and Z Schuss**[2]

[1] Group of Applied Mathematics and Computational Biology, IBENS,
Ecole Normale Supérieure, 46 rue d'Ulm, F-75005 Paris, France
[2] Department of Applied Mathematics, Tel-Aviv University, Tel-Aviv 69978, Israel

E-mail: david.holcman@ens.fr and schuss@post.tau.ac.il

Received 25 July 2013, revised 14 February 2014
Accepted for publication 17 February 2014
Published 9 April 2014

Abstract

Diffusion is the driver of critical biological processes in cellular and molecular biology. The diverse temporal scales of cellular function are determined by vastly diverse spatial scales in most biophysical processes. The latter are due, among others, to small binding sites inside or on the cell membrane or to narrow passages between large cellular compartments. The great disparity in scales is at the root of the difficulty in quantifying cell function from molecular dynamics and from simulations. The coarse-grained time scale of cellular function is determined from molecular diffusion by the mean first passage time of molecular Brownian motion to a small targets or through narrow passages. The narrow escape theory (NET) concerns this issue. The NET is ubiquitous in molecular and cellular biology and is manifested, among others, in chemical reactions, in the calculation of the effective diffusion coefficient of receptors diffusing on a neuronal cell membrane strewn with obstacles, in the quantification of the early steps of viral trafficking, in the regulation of diffusion between the mother and daughter cells during cell division, and many other cases. Brownian trajectories can represent the motion of a molecule, a protein, an ion in solution, a receptor in a cell or on its membrane, and many other biochemical processes. The small target can represent a binding site or an ionic channel, a hidden active site embedded in a complex protein structure, a receptor for a neurotransmitter on the membrane of a neuron, and so on. The mean time to attach to a receptor or activator determines diffusion fluxes that are key regulators of cell function. This review describes physical models of various subcellular microdomains, in which the NET coarse-grains the molecular scale to a higher cellular-level, thus clarifying the role of cell geometry in determining subcellular function.

Keywords: stochastic modeling, diffusion, asymptotic methods, Fokker–Planck equation, flux regulation, molecular trafficking, molecular biophysics
PACS numbers: 82.20.Uv, 82.39.−k, 02.30.Jr, 87.10.Ed, 02.50.Ga, 87.18.Sn, 87.19.lg, 82.20.−w, 02.50.Fz, 87.10.Mn

(Some figures may appear in colour only in the online journal)

Contents

1. Introduction 2
   1.1. References to section 1 5
2. Theory of stochastic chemical reactions in confined microdomains 6
   2.1. Flux regulation by receptor clustering in cellular biology 8
   2.2. Random search with switching between different states 9
   2.3. References to section 2 15
3. Diffusion on a crowded membrane and intracellular trafficking 16
   3.1. Diffusion on a membrane crowded with obstacles 17
   3.2. Trafficking and the delivery flux of vesicles in neurite outgrowth 20
   3.3. References to section 3 20
4. Physical virology: modeling the early steps of cell viral infection at the molecular level 21
   4.1. The cytoplasmic viral trafficking 21
   4.2. Stochastic description of viral trajectories 21
   4.3. Probability that a viral particle arrives alive at a nuclear pore 25
   4.4. The mean arrival time to a small nuclear pore 26
   4.5. Endosomal viral escape 26
   4.6. References to section 4 27
5. The NET in neurobiology and synaptic transmission 27
   5.1. A model of the synaptic current 29
   5.2. The mean and variance of the synaptic current I_s 30
   5.3. Leakage in a conductor of Brownian particles 32
   5.4. Regulation of flux in a neuronal spine neck and across a thin synaptic cleft 34
   5.5. References to section 5 37
6. Diffusion in composite domains 38
   6.1. Transition rate and the principal eigenvalue in composite domains 41
   6.2. The principal eigenvalue in a domain with a head and narrow neck 42
   6.3. The principal eigenvalue and coarse-grained diffusion in a dumbbell 43
   6.4. Diffusional transfer of genetic material during cell division 44
7. Summary and discussion 45
Acknowledgment 45
References 45

1. Introduction

Diffusion drives critical biological processes in cellular physiology, such as the search for a binding partner in biochemistry, the neuronal transmission in neurophysiology (Kandel *et al* 2000, Alberts *et al* 1994), the splitting of molecules (mRNA or proteins) between mother and daughter cells during cell division, and many other processes. The very different spatial and temporal scales in these processes are due to small binding sites inside or on the cell

boundary, or narrow passages between large compartments. The great disparity in scales in these examples is manifested as singular perturbation problems in their mathematical models. The quantification of the function of cellular microdomains from their geometrical structure, such as of neuronal synapses, falls in the class of multiple-scale problems of narrow escape theory (NET) (Holcman and Schuss 2014). The narrow escape time NET in diffusion theory is the mean first passage time (MFPT) of a Brownian trajectory to a small absorbing part of an otherwise reflecting boundary of a bounded domain. The renewed interest in the NET is due to its emergence as a key to the determination of biological cell function from its geometrical structure.

The physics of cell function has to be understood at the molecular level, which determines the dynamics of much larger cellular structures, such as the dynamics of molecular fluxes in microdomains and synapses (figure 14). Physical modeling on the cellular scale has serious pitfalls, because the temporal scale of cellular events is determined on the molecular level by refined details of cell structure, which cannot be captured in cellular-level models. This time scale has to be divined from a much lower-level model (see references in section 1.1). The behavior of molecules is complex not only because of their individual structure, but also because they form clusters or have specific interactions (see section 2.1).

Brownian dynamics simulations of molecular models often fail to capture the time scale of rare events, such as the passage of ions through protein channels of cellular membranes or the passage of molecules through narrow passages between cellular compartments. An analytical approach to the evaluation of the rate of rare events can lead to rational coarse-graining of the molecular model. For example, the analytical expression for the NET (Holcman and Schuss 2014) reduces the dimension of stochastic simulation data of exploration to that of the parameter space of the dynamics. It leads to an analytical expressions for an effective diffusion coefficient and for the rate of passage between compartments through necks. The narrow passage is especially important in quantifying the molecular searches that are not directed at long distances by a field of force and the only flux-control mechanism is the geometrical structure.

The development of molecular-level models follows a recent technological development of live-cell microscopy, which affords access to individual molecular trajectories on the surface of neuronal cells (Choquet and Borgdorff 2002, Borgdorff and Choquet 2002, Triller and Choquet 2003). Marked molecules provide short-time samples of trajectories that can be traced (Hoze *et al* 2010), therefore the reconstruction of their dynamics from the statistics of the samples is not an obvious task. The Brownian trajectories of the marked molecules cannot penetrate the cell membrane or other obstacles, but can be absorbed at receptors and other binding sites, or be terminated by a change of conformation or other chemical reactions, or when they exit the cell or a subcellular compartment and enter another structure. Different compartments for Brownian trajectories are often defined by the probability density of the observed trajectories or by the statistics of the time trajectories spend in a given spatial domain. By its very definition, the passage of a trajectory from one compartment to another is a rare event, which may be thermal activation over a potential barrier and/or (Holcman and Schuss 2004) traversing a narrow passage (Holcman and Schuss 2011), such as a channel, a single-file nano-pore, or a narrow neck.

Singular perturbation methods for the asymptotic analysis of the NET problem are reviewed in Holcman and Schuss (2014), where explicit expressions for NET are given. Approximate analytical and numerical solutions of the associated boundary value problems for the Pontryagin–Andronov–Vitt equation (Schuss 2010b, 2013) are derived for various geometries representing accessible and hidden single or multiple targets. The asymptotic methods are based on solving mixed Dirichlet–Neumann problems for elliptic and parabolic

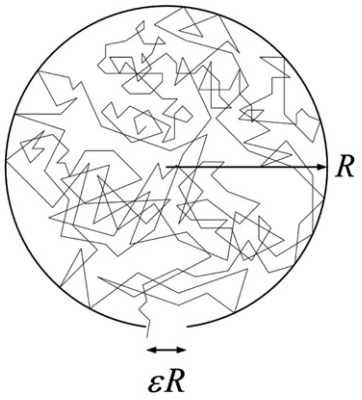

Figure 1. Brownian trajectory escaping through a small absorbing window of a domain with otherwise reflecting boundary.

equations using the singularity of the Neumann function (Singer *et al* 2008). The NET is also shown to be related to the principal eigenvalue of the mixed Dirichlet–Neumann problem for the Laplace equation in a domain, when the Dirichlet boundary is only a small patch on the otherwise Neumann boundary. As mentioned above, the principal eigenvalue is asymptotically the reciprocal of the NET in the limit of shrinking Dirichlet patch. In this limit the escape of a Brownian trajectory becomes a rare event and is thus hard to track by Brownian dynamics simulations due to the high computational complexity and to the high dimension of the parameter space. The explicit asymptotic approximation for the NET leads to the design of Brownian simulations of cellular processes, as described below. This review explains how to use these expressions to coarse-grain biophysical and biological models and to extract properties from newly available molecular data and from Brownian simulations.

The NET $\bar{\tau}$, that is, the MFPT of a Brownian trajectory from a compartment to an absorbing target (figure 1) or through a narrow passage, is a fundamental concept in the description of rare events. Specifically, in the limit of small target $\bar{\tau}$ increases indefinitely and the probability density function of the time spent in a compartment prior to termination or escape becomes exponentially distributed (Schuss *et al* 2007, Schuss 2010b, section 6.1)

$$p_{\bar{\tau}}(t) \sim \bar{\tau}^{-1} \exp\{-t/\bar{\tau}\}. \tag{1.1}$$

The exponential rate $\bar{\tau}^{-1}$ is therefore the flux into the absorbing target. In the case of crossing from one compartment to another through a narrow neck the crossing rate is $1/2\bar{\tau}$, where $\bar{\tau}$ is the MFPT to the stochastic separatrix (SS) between the compartments, the latter is the locus of initial points of a Brownian trajectory from which it ends up in one compartment or the other with equal probabilities (Schuss 2010a). The rate can represent the molecular flux into receptors or through intercellular passages, such as channels or necks and therefore determines cell functions, such as neuronal signaling and other key cell functions. The importance of the explicit computation of $\bar{\tau}$ in a given model consists in the drastic reduction in the dimension of Brownian dynamics simulations to that of the dimension of the parameter space of the analytical expression for the NET. This reduction coarse-grains molecular physical models into the micrometer scale of cellular or subcellular structure and function.

When the moving particle is initially positioned close to the target (inside the boundary layer), escape is characterized by the probability distribution of arrival times and not simply by the exponential tail of the distribution (Mattos *et al* 2012). In dimension two, the boundary layer

expansion can be computed explicitly (Singer *et al* 2006a), whereas short-time asymptotics are much harder to estimate (see, for example, the short-time asymptotics given in Schuss and Spivak (2005) for pure diffusion), because they requires the knowledge of all the eigenvalues of the problem. The full probability distribution of arrival times can be evaluated by heavy numerical simulations.

There are several examples where an anomalous diffusion model is needed to describe more refined properties of molecular motion. This is the case for the motion of a single monomer on a polymer chain (Amitai 2010, Amitai and Holcman 2013). In other cases, the size of a diffusing particle affects its motion (Barkai *et al* 2012), (see also experimental evidences in Tabei *et al* (2012) and Jeon *et al* (2011)). We refer to other reviews for specific discussion of anomalous diffusion (Hoefling and Franosch 2013).

This review presents several molecular and cellular, as well as biophysical models, which are based on the NET approximation. In this approximation the details of the geometrical structure are coarse-grained into single parameter, the reciprocal of the NET, which is the arrival rate at a small absorbing boundary. Recent progress is reported on coarse-graining molecular-level models to cellular scale and on their resolution. The coarse-grained models extract cell function from the cell's geometrical structure. The first section presents a theory of stochastic chemical reactions in confined microdomains, based on a Markov chain model. In this theory the mean by which a given number of binding sites are activated can be calculated. It also presents the search strategy of a Brownian particle that switches at random between two states, but can find a small target only when in one of the two. Section two presents a model for computing the effective diffusion coefficient on a membrane crowded with obstacles and some applications to receptor trafficking on the surface of a neuron. Section 3 presents several models for the molecular-level study of the successive steps of viral infection inside a cell. The mathematical model for the study of the mean escape time of a virus from an endosome uses stochastic dynamics to describe cytoplasmic trafficking and Markov jumps. The model defines the probability of a virus arrival at the nucleus in terms of the Fokker–Planck equation. The success of the early steps of viral trafficking determine the capacity for viral infection (Amoruso *et al* 2011). Section 4 presents several diffusion problems related to synaptic transmission that take place at the junction between two neurons (Cowan *et al* 2003, Kandel *et al* 2000). An asymptotic computation is shown of the probability that a receptor in the synaptic cleft binds a diffusing neurotransmitter (NT) (figure 14). A summary is given of diffusion laws inside composite domains, such as dendritic spines, which are fundamental microdomains in synaptic communication (figure 20). The laws are based on flux formulas that are also used in the context of diffusion between cells. Finally, a discussion is given of possible extensions of the NET methodology to other molecular and cellular questions.

1.1. References to section 1

The narrow escape problem in diffusion theory was considered first by Lord Rayleigh in Rayleigh (1945) and elaborated in Fabrikant (1989), 1991); the terminology NET was introduced in Singer *et al* (2006c). A recent review of early results on the NET problem with many biological applications is given in Bressloff and Newby (2013). A basic text on neuroscience is Kandel *et al* (2000), where the terminology used in this section is explained. The neuronal cleft is discussed in Alberts *et al* (1994, chapter 19) and Kandel *et al* (2000). The description of ionic channels, their selectivity, gating, and function is given in Sakmannn and Neher (2010) and Hille (2001) (see also the Nobel lecture (MacKinnon 2003)). The reconstruction of the spatial organization of proteins and ions that define the channel pore

from recordings of channel current–voltage characteristics is described in Chen *et al* (1997) and Burger *et al* (2007).

2. Theory of stochastic chemical reactions in confined microdomains

The need to simulate several interacting species in a microdomain is particularly useful in the context of calcium dynamics in neuronal synapses. The number of involved molecules is of the order of tens to hundreds, which are tracked with fluorescent dyes that drastically interfere with the reaction and diffusion processes. A similar situation arises in the simulation of synaptic transmission, starting with the arrival of NT molecules at receptors on the post-synaptic membrane.

A significant reduction of the simulation complexity is achieved by using the analytically computed neurotransmitter flux into the receptors, rather than simulating it. Analytical formulas are also used for quantifying diffusion in dendritic spines. Additional progress in modeling chemical reactions is achieved by replacing complex Brownian simulations with coarse-grained Markov chains by taking advantage of the fact that the arrival process of Brownian particles from a practically infinite continuum to an absorbing target is Poissonian. It is possible then to coarse-grain the binding and unbinding processes in microdomains into a Markov process, thus opening the way to full analysis of stochastic chemical reactions. This simulation circumvents the complex reaction–diffusion partial differential equations that are much harder to solve. A recent application of this Markovian approximation concerns some new predictions about the rate of molecular dynamics that underlie the spindle assembly checkpoint during cell division. Another reduction achieved by using the asymptotic analytical approximation to the NET is the verification of molecular dynamics simulations in domains that contain small passages or targets. The convergence of the simulation can be measured by the convergence of the statistics of rare events to that predicted by the analytical asymptotic approximation.

Traditional chemical kinetics, based on mass-action laws or reaction–diffusion equations, give an inappropriate description of the stochastic chemical reactions in microdomains, where only a small number of substrate and reactant molecules is involved. A reduced Markovian description of the stochastic dynamics of the binding and unbinding of molecules is given in Holcman and Schuss (2005) and applied in Dao Duc and Holcman (2010, 2012). Specifically, consider two finite species, the mobile reactant M that diffuses in a bounded domain Ω and the stationary substrate S (e.g., a protein) that binds M. The boundary $\partial\Omega$ of the domain Ω is partitioned into an absorbing part $\partial\Omega_a$ (e.g., pumps, exchangers, another substrate that forms permanent bonds with M, and so on) and a reflecting part $\partial\Omega_r$ (e.g., a cell membrane). In this model the volume of M is neglected. In terms of traditional chemical kinetics the binding of M to S follows the law

$$M + S_{\text{free}} \underset{k_b}{\overset{k_f}{\rightleftharpoons}} MS, \tag{2.1}$$

where k_f is the forward binding rate constant, k_b is the backward binding rate constant, and S_{free} is the unbound substrate. The model of the reaction assumes that the M molecules diffuse in Ω independently and when bound, are released independently of each other at exponential waiting times with rate k_{-1}.

To calculate the average number of unbound (or bound) sites in the steady state the following reduced model is used. The number $k(t)$ of unbound receptors at time t is a Markovian birth–death process with states $0, 1, 2, \ldots, \min\{M, S\}$ and transition rates

$\lambda_{k\to k+1} = \lambda_k$, $\lambda_{k\to k-1} = \mu = k_{-1}$. The boundary conditions are $\lambda_{S\to S+1} = 0$ and $\lambda_{0\to -1} = 0$. Setting $P_k(t) = \Pr\{k(t) = k\}$, the Kolmogorov equations for the transition probabilities are given by Holcman and Schuss (2005)

$$\dot{P}_k(t) = -[\lambda_k + k_{-1}(S-k)]P_k(t) + \lambda_{k+1}P_{k+1}(t) + k_{-1}(S-k+1)P_{k-1}(t) \qquad (2.2)$$
$$\text{for} \quad k = (S-M)^+ + 1, \ldots, S-1$$

with the boundary equations

$$\dot{P}_{(S-M)^+}(t) = -k_{-1}SP_{(S-M)^+}(t) + \lambda_1 P_{(S-M)^+ +1}(t)$$
$$\dot{P}_S(t) = -\lambda_S P_S(t) + k_{-1}P_{S-1}(t)$$

and initial condition $P_{k,q}(0) = \delta_{k,S}\delta_{q,0}$. In the limit $t \to \infty$ the model (2.2) gives the average number

$$\langle k_\infty \rangle = \sum_{j=(S-M)^+}^{S} jP_j,$$

where $P_j = \lim_{t\to\infty} P_j(t)$. Similarly, the stationary variance of the number of unbound sites is $\sigma^2(M,S) = \langle k_\infty^2 \rangle - \langle k_\infty \rangle^2$, where $\langle k_\infty^2 \rangle = \sum_{j=(S-M)^+}^{S} j^2 P_j$.

The rates λ_k are modeled as follows. For a single diffusing molecule, the time to binding is the first passage time to reach a small absorbing portion $\partial\Omega_a$ of the boundary, which represents the active surface of the receptor, whereas the remaining part of $\partial\Omega$ is reflecting. Due to the small target and to the deep binding potential well the binding and unbinding of M to S are rare events on the time scale of diffusion (Schuss *et al* 2007). This implies that the probability distribution of binding times is approximately exponential (Schuss 2010b) with rate $\lambda_1 = 1/\mathbb{E}\tau_1$, where the NET $\mathbb{E}\tau_1$ is the MFPT to $\partial\Omega_a$. When there are S binding sites, $k(t)$ of which are unbound, there are $N = [M - S + k]^+$ free diffusing molecules in Ω, where $x^+ = \max\{0, x\}$. The arrival time of a molecule to the next unbound site is well approximated by an exponential law with state-dependent instantaneous rate (see discussion in Holcman and Schuss 2005)

$$\lambda_k = \frac{Nk}{\mathbb{E}\tau_1} = \frac{k(M-S+k)^+}{\mathbb{E}\tau_1}.$$

The results of the Markovian model (2.2) are

$$P_S = \frac{1}{1 + \sum_{k=1}^{S-(S-M)^+} \frac{\prod_{i=S-k+1}^{S} \mathrm{i}(M-S+i)^+}{k!(\mathbb{E}\tau_1 k_{-1})^k}}$$

$$\langle k_\infty \rangle = P_S \sum_{k=S-1}^{(S-M)^+} (S-k)^+ \frac{\prod_{i=S-k+1}^{S} \mathrm{i}(M-S+i)^+}{k!(\mathbb{E}\tau_1 k_{-1})^k}$$

$$\langle k_\infty^2 \rangle = P_S \sum_{k=S-1}^{(S-M)^+} [(S-k)^+]^2 \frac{\prod_{i=S-k+1}^{S} \mathrm{i}(M-S+i)^+}{k!(\mathbb{E}\tau_1 k_{-1})^k}$$

$$\sigma_S^2(M) = \langle k_\infty^2 \rangle - \langle k_\infty \rangle^2 \qquad (2.3)$$

(see Holcman and Schuss (2005) for further details).

These formulas are used to estimate the fraction of bound receptors in photo-receptor outer segments and also to interpret the channel noise measurements variance in Holcman and Schuss (2005). In Holcman and Triller (2006) this analysis was used to estimate the number of bound AMPA receptors in the post-synaptic density (PSD). A similar gated Markovian model was proposed in Bressloff and Earnshaw (2009). The reduced Markovian model is used for the

calculation of the mean time of the number of bound molecules to reach a given threshold T (MFTT). In a cellular context, the MFTT can be used to characterize the stability of chemical processes, especially when they underlie a biological function. Using the above Markov chain description, the MFTT can be expressed in terms of fundamental parameters, such as the number of molecules, of ligands, and the forward and backward binding rates. It turns out that the MFTT depends nonlinearly on the threshold T. Specifically, consider M Brownian molecules that can bind to immobile targets S inside a microdomain, modeled generically by equation (2.1). The first time the number $[MS](t)$ of MS molecules at time t reaches the threshold is defined as

$$\tau_T = \inf\{t > 0 : [MS](t) = T\} \tag{2.4}$$

and its expected value is $\bar{\tau}_T$. Consider the case of an ensemble of the targets initially free and distributed on the surface of a closed microdomain and assume that the backward rate vanishes ($k_{-1} = 0$) and $k_f > 0$. The dynamical system for the transition probabilities of the Markov process $MS(t)$ is similar to that above, but for the absorbing boundary condition at the threshold T, which gives (2.2) (Dao Duc and Holcman 2010). When the binding is irreversible ($k_{-1} = 0$), $\bar{\tau}_T$ is the sum of the forward rates

$$\begin{aligned}\tau_T^{\text{irrev}} &= \frac{1}{\lambda_0} + \frac{1}{\lambda_1} + \cdots + \frac{1}{\lambda_{T-1}} \\ &= \frac{1}{\lambda}\sum_{k=0}^{T-1} \frac{1}{(M_0 - k)(S_0 - k)}.\end{aligned} \tag{2.5}$$

In particular, when $M_0 = S_0$ and $M_0 \gg 1$, (2.5) becomes asymptotically $\tau_T^{\text{irrev}} \approx T/\lambda M_0(M_0 - T)$. In addition, when the number of diffusing molecules largely exceed the number of targets ($M_0 \gg S_0, T$), (2.5) gives the asymptotic formulas

$$\tau_T^{\text{irrev}} \approx \begin{cases} \dfrac{1}{\lambda M_0} \log \dfrac{S_0}{S_0 - T} & \text{for} \quad M_0 \gg S_0, T \\ \dfrac{1}{\lambda S_0} \log \dfrac{M_0}{M_0 - T} & \text{for} \quad S_0 \gg M_0, T \\ \dfrac{T}{\lambda M_0 S_0} & \text{for} \quad M_0, S_0 \gg T. \end{cases} \tag{2.6}$$

Figure 2 shows the plot of τ_T^{irrev} for several values of the threshold T, compared to Brownian simulations in a circular disk $\Omega = D(R)$ with reflecting boundary, except at the targets.

2.1. Flux regulation by receptor clustering in cellular biology

There are several studied examples, where changing the arrangement of absorbing windows affects the cell function. In bacteria, receptors re-cluster, depending on the external concentration of a chemotactic attractant, thus improving the sensitivity. In the context of neuroscience, receptors are known to re-cluster before the tip of a growing neuron (growth cone) turns toward a chemoattractant. Changing the arrangement of AMPA receptors in neuronal synapses affects the synaptic transmission. The variations in the shape of dendritic spines of neurons as a result of learning and other physiological activities changes both the density and distribution of receptors, transporters and other regulatory proteins, thereby changing the ionic flux through the membrane. Thus calcium dynamics in dendritic spines can be controlled at the cellular level by rearrangement of channels and exchangers.

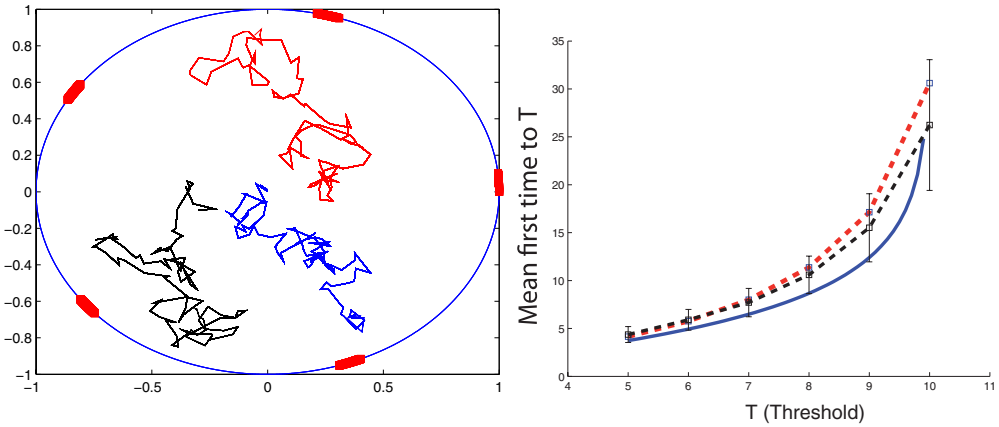

Figure 2. The MFTT. Left: trajectories of diffusing molecules in a microdomain containing five binding sites on the boundary. Right: the time τ_T^{irrev} is plotted as a function of the threshold T. Brownian simulations (dotted blue line, variance in black), the theoretical formula (2.5) (dotted red line) and its approximation (2.6) (continuous blue line) for a circular disk in the irreversible case ($k_{-1} = 0$). The other parameters are $S_0 = 15$, $M_0 = 10$, $\varepsilon = 0.05$, $D = 0.1\,\mu\text{m}^2\text{s}^{-1}$ and the radius of the disk $R = 1\,\mu\text{m}$ (200 runs).

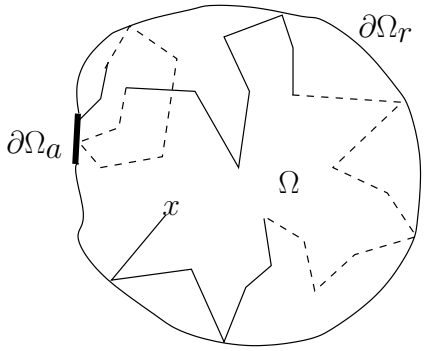

Figure 3. Example of a trajectory of a diffusing Brownian ligand in a confined domain Ω and randomly switching between two states 1 (continuous line) and 2 (dashed line). In state 2, the ligand is reflected all over the boundary, while in state 1 it is absorbed at $\partial\Omega_a$.

2.2. Random search with switching between different states

Consider Brownian motion in a bounded domain Ω, whose diffusion coefficient is a random telegraph signal that switches between two values, D_1 and D_2, at exponential waiting times with rates k_{12} and k_{21}, respectively (see figure 3). When the diffusion coefficient is D_1, the Brownian trajectory is reflected in the boundary $\partial\Omega$, except for a small absorbing part $\partial\Omega_a$. When the diffusion coefficient is D_2, the entire boundary reflects the Brownian trajectory. The gated narrow escape time (GNET) is the time to absorption of the switching Brownian trajectory and the mean time to absorption is the GNET. More generally, a class of diffusions is considered that switch between different diffusion coefficients $D_1, \ldots, D_n$ at exponential waiting times with given rates k_{ij} and are absorbed at a small part $\partial\Omega_a$ of $\partial\Omega$ while in states $D_1, \ldots, D_k$ and are otherwise reflected in $\partial\Omega$. The GNET is related to certain intermittent

search processes, where switching strategies between different states lead to minimal search time of a target (Bénichou *et al* 2005). Other switching searches have been investigated where a stochastic particle moves close to the surface membrane (Tsaneva *et al* 2009, Oshanin *et al* 2010, Berezhkovskii and Barzykin 2012).

The gated narrow escape model is used to calculate the GNET, which requires the solution of a coupled system of mixed Dirichlet–Neumann boundary value problems for Poisson's equations. The system was recently solved in Reingruber and Holcman (2009, 2010).

2.2.1. Random switching between two modes of diffusion. Consider stochastic dynamics $\boldsymbol{x}(t, i)$ that switches between two states, $i = 1$ and $i = 2$ (e.g., due to change of conformation), at exponential waiting times with rates k_{12} and k_{21}, respectively, and diffuses in state i with diffusion constant D_i. Its Euler simulation for $t > s$ is given by

$$\boldsymbol{x}(t + \Delta t, i) = \begin{cases} \boldsymbol{x}(t, i) + \sqrt{2D_i}\Delta \boldsymbol{w}_i(t) & \text{w.p.} \quad 1 - k_{ij}\Delta t + o(\Delta t) \\ \\ \boldsymbol{x}(t, j) & \text{w.p.} \quad k_{ji}\Delta t + o(\Delta t), \ i \neq j \end{cases} \tag{2.7}$$

for $i, j = 1, 2$, with an initial condition $\boldsymbol{x}(s, i) = \boldsymbol{x}$, in which the states $i = 1$ and $i = 2$ can be randomly distributed. Here $\boldsymbol{w}_i(t)$ $(i = 1, 2)$ are independent standard Brownian motions and $\Delta \boldsymbol{w}_i(t) = \boldsymbol{w}_i(t + \Delta t) - \boldsymbol{w}_i(t)$.

The transition probability density function $p(\boldsymbol{y}, i, t \,|\, \boldsymbol{x}, s, j)$ of the trajectory $x(t, i)$ in a given domain Ω, given the initial condition $\boldsymbol{x}(s, j) = \boldsymbol{x}$ with probability 1, is the limit as $\Delta t \to 0$ of the solution to the system of integral equations (Schuss 2010b)

$$p(\boldsymbol{y}, i, t + \Delta t \,|\, \boldsymbol{x}, s, j) = \frac{1 - k_{ij}\Delta t}{\sqrt{2\pi D_i \Delta t}} \int_\Omega p(\boldsymbol{z}, i, t \,|\, \boldsymbol{x}, s, j) \exp\left\{-\frac{|\boldsymbol{y} - \boldsymbol{z}|^2}{2D_i \Delta t}\right\} \mathrm{d}\boldsymbol{z}$$
$$+ k_{ji}\Delta t\, p(\boldsymbol{y}, \ell, t \,|\, s, j) + o(\Delta t) \ \text{ for } \ i, j, \ell = 1, 2, \ i \neq \ell.$$

In the limit $\Delta t \to 0$, the system of Kolmogorov (master) equations is obtained

$$p_t(\boldsymbol{y}, 1, t \,|\, \boldsymbol{x}, s) = D_1 \Delta_y p(\boldsymbol{y}, 1, t \,|\, \boldsymbol{x}, s) - k_{12} p(\boldsymbol{y}, 1, t \,|\, \boldsymbol{x}, s) + k_{12} p(\boldsymbol{y}, 2, t \,|\, \boldsymbol{x}, s)$$
$$p_t(\boldsymbol{y}, 2, t \,|\, \boldsymbol{x}, s) = D_2 \Delta_y p(\boldsymbol{y}, 2, t \,|\, \boldsymbol{x}, s) + k_{21} p(\boldsymbol{y}, 1, t \,|\, \boldsymbol{x}, s) - k_{21} p(\boldsymbol{y}, 2, t \,|\, \boldsymbol{x}, s), \tag{2.8}$$

which can be easily generalized to any number of states (Reingruber and Holcman 2010). Setting

$$\boldsymbol{p} = \begin{pmatrix} p(\boldsymbol{y}, 1, t \,|\, \boldsymbol{x}, s) \\ p(\boldsymbol{y}, 2, t \,|\, \boldsymbol{x}, s) \end{pmatrix}, \quad \boldsymbol{K} = \begin{pmatrix} k_{12} & -k_{12} \\ -k_{21} & k_{21} \end{pmatrix}, \quad \boldsymbol{D}_y = \begin{pmatrix} D_1 & 0 \\ 0 & D_2 \end{pmatrix} \Delta_y,$$

the forward master equations (2.8) can be written as

$$\boldsymbol{p}_t(\boldsymbol{y}, t \,|\, \boldsymbol{x}, s) = \boldsymbol{D}_y \boldsymbol{p}(\boldsymbol{y}, t \,|\, \boldsymbol{x}, s) - \boldsymbol{K}\boldsymbol{p}(\boldsymbol{y}, t \,|\, \boldsymbol{x}, s). \tag{2.9}$$

The transition probability density function $\boldsymbol{p}\,(\boldsymbol{y}, t \,|\, \boldsymbol{x}, s)$ satisfies the backward system of master equations (with respect to $(\boldsymbol{x}, s)$), which is the formal adjoint to (2.9). Upon setting $t - s = \tau$, as we may, we obtain

$$\boldsymbol{p}_\tau(\boldsymbol{y}, \tau \,|\, \boldsymbol{x}, 0) = \boldsymbol{D}_x \boldsymbol{p}(\boldsymbol{y}, \tau \,|\, \boldsymbol{x}, 0) - \boldsymbol{K}^T \boldsymbol{p}(\boldsymbol{y}, \tau \,|\, \boldsymbol{x}, 0). \tag{2.10}$$

The mean sojourn time in state i prior to absorption, $u(i \,|\, \boldsymbol{x}, 1)$, of a trajectory of (2.7) that starts at $\tau = 0$ in state 1 at position $\boldsymbol{x}$ with probability 1, is given by Schuss (2010b)

$$u(i \,|\, \boldsymbol{x}, 1) = \int_\Omega \mathrm{d}\boldsymbol{y} \int_0^\infty \mathrm{d}\tau\, p(\boldsymbol{y}, i, \tau \,|\, \boldsymbol{x}, 1). \tag{2.11}$$

To find the differential equations that the times $u(i \,|\, \boldsymbol{x}, j)$ satisfy, the backward equation (2.10) is integrated with respect to $\boldsymbol{y}$ and τ to obtain

$$D_1 \Delta u(i \,|\, \boldsymbol{x}, 1) - k_{12}[u(i \,|\, \boldsymbol{x}, 1) - u(i \,|\, \boldsymbol{x}, 2)] = -1$$
$$D_2 \Delta u(i \,|\, \boldsymbol{x}, 2) - k_{21}[u(i \,|\, \boldsymbol{x}, 2) - u(i \,|\, \boldsymbol{x}, 1)] = 0.$$

The mean sojourn times $u(2\,|\,\boldsymbol{x}, 1)$ and $u(2\,|\,\boldsymbol{x}, 2)$ satisfy equations that are obtained by interchanging $1 \leftrightarrow 2$ in (2.12). It suffices to solve the equations only for $i = 1$, because the solutions $u(2\,|\,\boldsymbol{x}, j)$ can be obtained from $u(1\,|\,\boldsymbol{x}, j)$ by linear transformations. Specifically, averaging $u(i\,|\,\boldsymbol{x}, j)$ over a uniform initial spatial distribution of $\boldsymbol{x}$, we define the mean sojourn times prior to absorption as

$$u(i\,|\,j) = \frac{1}{|\Omega|}\int_\Omega u(i\,|\,\boldsymbol{x}, j)\,\mathrm{d}\boldsymbol{x}. \tag{2.13}$$

When the trajectory $\boldsymbol{x}(t, i)$ is absorbed at $\partial\Omega_a$ with $i = 1$ while it is reflected everywhere on the $\partial\Omega$ with $i = 2$, the boundary conditions for the system (2.12) are

$$u(1\,|\,\boldsymbol{x}, 1) = 0 \ \text{ for } \ \boldsymbol{x} \in \partial\Omega_a, \quad \frac{\partial u(1\,|\,\boldsymbol{x}, 1)}{\partial n} = 0 \ \text{ for } \ \boldsymbol{x} \in \partial\Omega_r,$$
$$\frac{\partial u(1\,|\,\boldsymbol{x}, 2)}{\partial n} = 0 \ \text{ for } \ \boldsymbol{x} \in \partial\Omega.$$

The sojourn times $u(2\,|\,\boldsymbol{x}, 1)$ and $u(2\,|\,\boldsymbol{x}, 2)$ are obtained from $u(1\,|\,\boldsymbol{x}, 1)$ and $u(1\,|\,\boldsymbol{x}, 2)$ through the linear transformation

$$\begin{pmatrix} u(2\,|\,\boldsymbol{x}, 1) \\ u(2\,|\,\boldsymbol{x}, 2) \end{pmatrix} = \frac{k_{12}}{k_{21}}\begin{pmatrix} 1 & 0 \\ 0 & 1 \end{pmatrix}\begin{pmatrix} u(1\,|\,\boldsymbol{x}, 1) \\ u(1\,|\,\boldsymbol{x}, 2) \end{pmatrix} + \begin{pmatrix} 0 \\ 1/k_{21} \end{pmatrix}. \tag{2.14}$$

Equations (2.12) and (2.14) show that the spatially averaged sojourn times (2.13) satisfy the relations

$$u(1\,|\,2) = u(1\,|\,1), \quad u(2\,|\,1) = u(1\,|\,1)\frac{k_{12}}{k_{21}}, \quad u(2\,|\,2) = u(2\,|\,1) + \frac{1}{k_{21}}. \tag{2.15}$$

It follows that the mean sojourn times $u(1)$, $u(2)$, and u, conditioned on a uniform initial distribution in states 1, 2, or in 1 and 2 with the equilibrium distribution $(p_1, p_2) = (k_{21}, k_{12})/(k_{12} + k_{21})$, respectively, are

$$\begin{aligned} u(1) &= u(1\,|\,1) + u(2\,|\,1) = u(1\,|\,1)\left(1 + \frac{k_{12}}{k_{21}}\right) \\ u(2) &= u(2\,|\,2) + u(2) = u(1) + \frac{1}{k_{21}} \\ u &= p_1 u(1) + p_2 u(1\,|\,2) = u(1) + \frac{p_2}{k_{21}}. \end{aligned} \tag{2.16}$$

2.2.2. GNET in one dimension. The GNET for one-dimensional diffusion, though not directly relevant to biological applications, can be calculated explicitly (Reingruber and Holcman 2009, 2010) and is quite instructive about the dependence of the NET on switching. Specifically, the system (2.12) in the interval $\Omega = (0, L)$ with absorption at $x = 0$ in state 1 and reflection at $x = L$ is given in the scaled variables

$$\begin{aligned} &\hat{x} = \frac{x}{L}, \quad l_1 = \frac{k_{12}L^2}{D_1}, \quad l_2 = \frac{k_{21}L^2}{D_2} \\ &\kappa = \frac{D_1}{D_2}, \quad v_1(\hat{x}) = \frac{D_1}{L^2}u_1(x, 1), \quad v_2(\hat{x}) = \frac{D_1}{L^2}u_1(x, 2) \end{aligned} \tag{2.17}$$

by

$$v_1''(\hat{x}) - l_1[v_1(\hat{x}) - v_2(\hat{x})] = -1, \quad v_2''(\hat{x}) + l_2[v_1(\hat{x}) - v_2(\hat{x})] = 0, \tag{2.18}$$

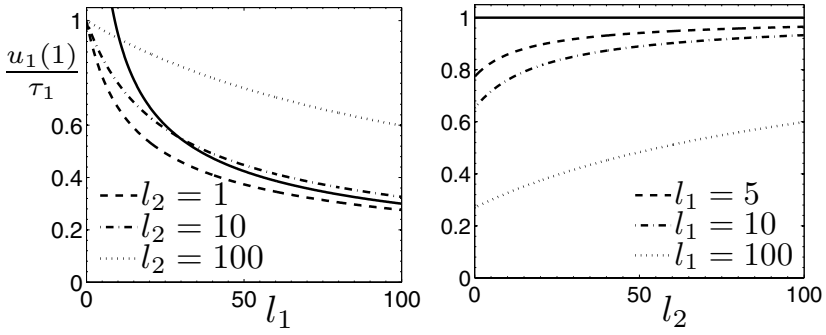

Figure 4. Graph of the sojourn time $u(1\,|\,1)$ obtained from the explicit solution as a function of l_1 (left) and l_2 (right), scaled by the NET τ_1 with no switching. The continuous curve in the left panel is the asymptotic approximation $3/\sqrt{l_1}$ for $l_1 \gg 1$ and $\sqrt{l_1} \gg l_2$.

with boundary conditions $v_1(0) = v_1'(1) = v_2'(0) = v_2'(1) = 0$, which can be solved explicitly. The nonlinear effect of switching can be seen from the explicit expressions

$$u(1\,|\,1) = \begin{cases} \dfrac{L^2}{D_1}\left[\dfrac{\coth\sqrt{l_1}}{\sqrt{l_1}} - \dfrac{1}{l_1}\right] + O\left(\dfrac{l_2}{l_1}\right), & \text{for } l_2 \ll l_1 \\ \dfrac{L^2}{3D_1} + O\left(\dfrac{l_1}{l_2}\right), & \text{for } l_2 \gg l_1, \end{cases} \tag{2.19}$$

while for $l_1 \gg 1$ and $l_2 \ll \sqrt{l_1}$

$$u(1\,|\,1) \approx \frac{L^2}{D_1}\frac{1}{\sqrt{l_1}} = \frac{L}{\sqrt{k_{12}D_1}}, \quad l_1 \gg 1, \sqrt{l_1} \gg l_2. \tag{2.20}$$

Figure 4 shows the plots of $u(1\,|\,1)$ versus l_1 (left) and versus l_2 (right). The counterintuitive result, that the sojourn time $u(1\,|\,1)$ is always smaller than the mean exit time in state 1 without switching, is remarkable. In addition, when the parameters D_1, D_2, and k_{21} are fixed, (2.20) shows that $u(1\,|\,1)$ becomes arbitrarily small as k_{12} increases. This counter intuitive behavior can be understood as follows (see also Doering (2000)). For a trajectory starting uniformly distributed in state 1, the probability to be in the neighborhood of the absorbing boundary at $x = 0$ decreases quickly as a function of time. However, after switching to state 2, the distribution is re-homogenized and later on, after switching back to state 1, the probability density around $x = 0$ is higher than that in the non-switching case. After switching back to state 1, the ligand starts closer to $x = 0$ with high probability and thus exits in state 1 faster than in the non-switching case. Figure 5 (left) shows the plot of $u(1)$ versus l_1 for various fixed values of l_2. This situation describes a chemical reaction, where the diffusion constants and the backward rate k_{21} are fixed, but the forward binding rate k_{12} can be adjusted by changing the concentration of a reactant partner. Figure 5 (right) shows the plot of $u(1)$ versus l_2 for fixed l_1, which demonstrates that also $u(1)$ has a minimum $u(1)_m$ in this case. The minimum $u(1)_m$ decreases as switching becomes faster. A lower bound for $u(1)_m$ can also be found explicitly. The analysis of the one-dimensional case shows that the lower limit of the GNET $u(1)$ corresponds to diffusion with the maximal diffusion constant and for $\kappa = D_1/D_2 \leqslant 1$, the fastest exit is achieved by diffusing most of the time in state 2, with no exits possible. The exit time $u(1)$ has no global or even local minima for $\kappa < 1$ and the best strategy to minimize the GNET needs to be adapted to the given constraints. For example, when k_{21} k_{12} are the unbinding and the binding rates, respectively, k_{21} usually depends on the local interaction

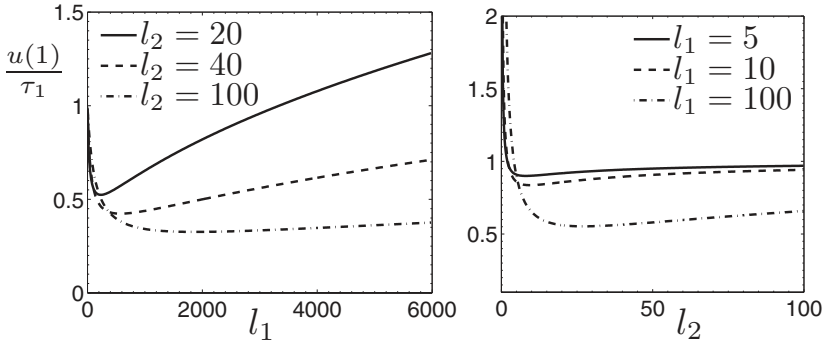

Figure 5. Graph of the exit time $u(1)$ as a function of l_1 (left) and l_2 (right) for $D_1/D_2 = 0.1$, scaled by NET τ_1 in the absence of switching.

potential while k_{12} can be modulated by changing the concentration of the binding partner. Furthermore, as shown in figure 5, the graph of $u(1)$ around and past the minimum is quite flat, and thus increasing switching to attain the minimum may not be necessary, because a similar effect can already by achieved at much slower rates. Moreover, because the graph of $u(1)$ decays steeply for small values l_1 and l_2, this behavior provides an efficient mechanism to modulate the activation time, and thus modulate cellular signaling.

2.2.3. GNET in three dimensions. Consider the GNET problem for a three-dimensional domain Ω when the trajectory is absorbed upon hitting $\partial\Omega_a$ in state 1 only. In the absence of switching, the time reduces to the NET τ_1 (Kolokolnikov *et al* 2005, Singer *et al* 2006b, Grigoriev *et al* 2002), which shows that outside a small boundary layer around the absorbing hole of radius a, where a characterizes the extent of $\partial\Omega_a$, the positional NET is almost independent of the initial ligand position (Singer *et al* 2006b). Using the scaling (Reingruber *et al* 2009)

$$\hat{\boldsymbol{x}} = \frac{\boldsymbol{x}}{a}, \quad l_1 = \frac{k_{12}a^2}{D_1}, \quad l_2 = \frac{k_{21}a^2}{D_2}, \quad v_1(\hat{\boldsymbol{x}}) = \frac{aD_1}{|\Omega|}u_1(\boldsymbol{x}, 1), \quad v_2(\hat{\boldsymbol{x}}) = \frac{aD_1}{|\Omega|}u_1(\boldsymbol{x}, 2),$$

the equations (2.12) become the dimensionless system

$$\begin{aligned} &\Delta v(\mathrm{i}|\hat{\boldsymbol{x}}, 1) - l_1[v(\mathrm{i}\,|\,\hat{\boldsymbol{x}}, 1) - v(\mathrm{i}\,|\,\hat{\boldsymbol{x}}, 2)] = -|\hat{\Omega}|^{-1} \\ &\Delta v(\mathrm{i}\,|\,\hat{\boldsymbol{x}}, 2) + l_2[v(\mathrm{i}\,|\,\hat{\boldsymbol{x}}, 1) - v(\mathrm{i}\,|\,\hat{\boldsymbol{x}}, 2)] = 0, \end{aligned} \tag{2.21}$$

where $|\hat{\Omega}| = |\Omega|/a^3 \gg 1$. The boundary conditions are absorbing on $\partial\hat{\Omega}_a$ for $v_1(\hat{\boldsymbol{x}})$, and otherwise reflecting. Asymptotic approximations to the solution of (2.21) in the limit of small window and extreme values of the parameters clarify the effect of switching. For $l_1 \ll 1$ or $l_2 \gg l_1$, at leading orders, $v(1\,|\,\hat{\boldsymbol{x}}, 1)$ is the solution of the NET problem $\Delta v(1\,|\,\hat{\boldsymbol{x}}, 1) = -|\hat{\Omega}|^{-1}$. When $l_2 \ll \sqrt{l_1}$, the leading order approximation for $v(1\,|\,\hat{\boldsymbol{x}}, 1)$ is found by solving $\Delta v(1\,|\,\hat{\boldsymbol{x}}, 1) - l_1[v(1\,|\,\hat{\boldsymbol{x}}, 1) - v_1] = -|\hat{\Omega}|^{-1}$, where v_1 is the spatial average of $v(1\,|\,\hat{\boldsymbol{x}}, 1)$. The leading order asymptotic approximation to the mean sojourn time is

$$u(1) = \left(1 + \frac{k_{12}}{k_{21}}\right)\frac{|\Omega|}{aD_1}v_1 \tag{2.22}$$

$$\sim \left(1 + \frac{k_{12}}{k_{21}}\right)\begin{cases} \tau_1 & \text{for } l_1 \ll 1 \text{ or } l_2 \gg l_1 \\ \dfrac{|\Omega|}{|\partial\Omega_a|\sqrt{D_1 k_{12}}} & \text{for } l_1 \gg 1,\ \sqrt{l_1} \gg l_2, \end{cases} \tag{2.23}$$

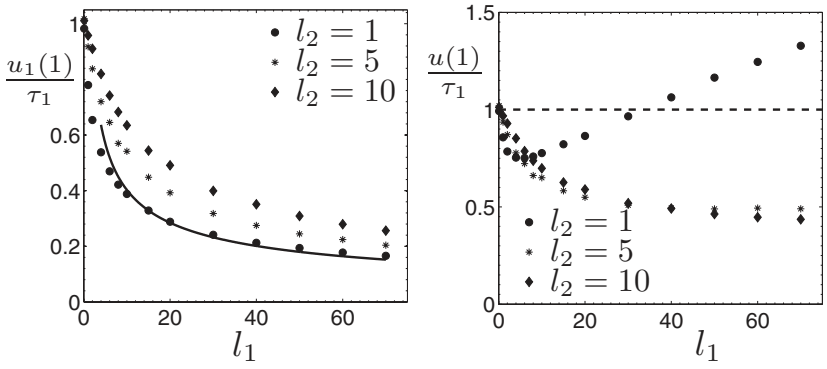

Figure 6. Simulation results for the mean sojourn time $u(1\,|\,1)$ and the mean exit time $u(1)$ as a function of l_1 for different values of l_2 (marked by various symbols). The results are scaled by the NET τ_1. The continuous line in the left panel is the asymptotic value $4/\pi\sqrt{l_1}$, obtained from (2.23) (see text). The results for $u(1)$ in the right panel are obtained for $\kappa = 0.1$.

where τ_1 is the NET in state 1 without switching. The asymptotic behavior (2.23) of $u(1)$ and $u(1\,|\,1)$ as functions of l_1 and l_2 is confirmed by Brownian simulations together with the Gillespie-algorithm (Gillespie 1976) to model switching in a sphere of radius $r = 30$ with a circular hole of radius $a = 1$. In the left panel of figure 6 simulation results are shown for $u(1\,|\,1)$ as a function of l_1 for various values of l_2. Clearly, $u(1\,|\,1) \leqslant \tau_1$, which confirms the asymptotic behavior $u(1\,|\,1)/\tau_1 \approx 4/(\pi\sqrt{l_1})$. The latter follows from (2.23) with the asymptotic approximation $\tau_1 \approx |\Omega|/(4aD_1)$ (Schuss *et al* 2007) and $|\partial\Omega_a| = \pi a^2$. Simulations results for $u(1)$ as a function of l_1 for various values of l_2 and $\kappa = 0.1$ ($D_1 = 1, D_2 = 10$) are displayed in the left panel of figure 6. The plot shows that $u(1)$ has a minimum $u(1)_m$ smaller than τ_1, which is attained at some value $l_{1,\min} > 0$.

In the range of parameters such that $u_1(1) \approx \tau_1$ the switching dynamics can be approximated by an effective non-switching diffusion process with diffusion constant $D_{\text{eff}} = D_1/(1 + k_{12}/k_{12})$. However, because $D_{\text{eff}} < D_1$, the effective diffusion approximation cannot give an exit time $u(1)$ smaller than τ_1. Interestingly, (2.23) shows that $u(1)$ in the range $\sqrt{l_1} \gg l_2, l_1 \gg 1$ is smaller than τ_1 and inversely proportional to the surface area of the absorbing window, similarly to the NET to a partially absorbing hole (Reingruber *et al* 2009). In this range, the switching dynamics cannot be approximated by the classical diffusion process. If $D_2 > D_1$, then switching can significantly decrease the GNET relative to the non-switching NET. For small values of l_1 and l_2, the GNET is very sensitive to changes in these parameters (see figures 5 and 6).

2.2.4. Application to the transcription factor search. The above computations of the GNET are relevant to a transcription factor (TF) search time for a DNA-promoter site (figure 7). The search can alternate between three-dimensional diffusion in the nucleus and one-dimensional diffusion along the DNA (figure 8) (Elf *et al* 2007, Wang *et al* 2006, Von Hippel and Berg 1989). While diffusing along the DNA, the TF can switch at random between two conformational states: in state 1 the diffusion is slow due to a high affinity of the TF for the DNA and therefore it scans accurately the DNA base pairs. In state 2, diffusion is much faster, but the TF does not scan the DNA molecule accurately. It was shown recently that the search time of such a TF can be significantly reduced relative to that of a TF, which accurately examines all the

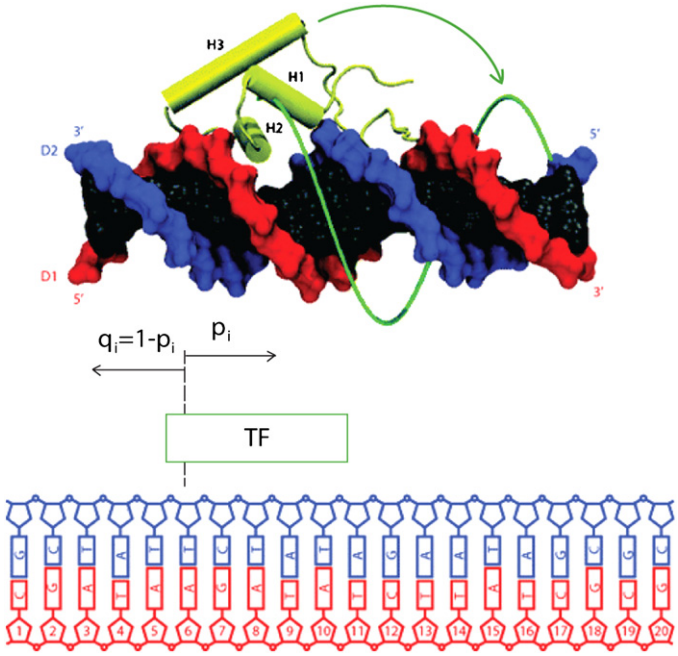

Figure 7. Motion of a TF along the DNA molecule. A TF located at position i moves by one base pair to the right with a probability p_i and to the left with a probability q_i as represented in the lower half of the figure (Malherbe and Holcman 2010). Figure adapted from Furini *et al* (2010). With permission from Furini *et al* 2010 *J. Phys. Chem.* B **114** 2238–45. Copyright (2010) American Chemical Society.

DNA base pairs. Several recent computations show that the mean time to find the DNA site is several minutes long (Malherbe and Holcman 2010, Reingruber and Holcman 2011b). The following opens fundamental question that remains to be addressed: what is the role of DNA conformation, accessibility, and chromatin organization in the search process?

2.3. References to section 2

Simulations of several interacting species in a microdomain were reported in Holcman *et al* (2004). Synaptic transmission, starting with the arrival of NT molecules at receptors on the post-synaptic membrane were reported in Freche *et al* (2011), Taflia and Holcman (2011), Holcman and Triller (2006), and Reingruber and Holcman (2011a). Quantification of diffusion in dendritic spines was reported in Biess *et al* (2007). A simplified model of chemical reaction simulations was achieved in Holcman and Schuss (2005) and Dao Duc and Holcman (2010) by replacing Brownian simulations with coarse-grained Markov chains. A key feature here is the fact that the arrival process of Brownian particles from a practically infinite continuum to an absorbing target is Poissonian (Nadler *et al* 2002, Schuss *et al* 2007). A reduced Markovian description of the stochastic dynamics of the binding and unbinding of molecules is given in Holcman and Schuss (2005) and applied in Dao Duc and Holcman (2010, 2012). Spindle assembly checkpoint during cell division was studied in Dao Duc and Holcman (2012). Verification of molecular dynamics simulations in domains that contain small passages or targets was done in Biess *et al* (2007).

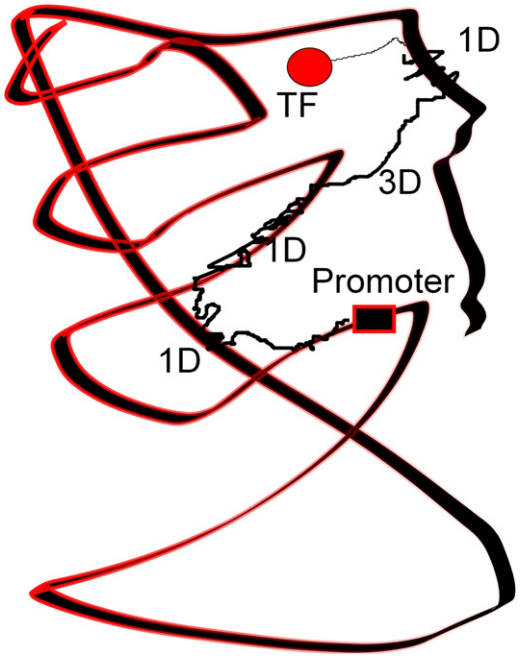

Figure 8. Search scenario for a DNA target by a TF. The TF can attach to the DNA molecule and scan a number of potential binding sites or diffuse freely in the nucleus. The TF alternates periods of one-dimensional random walks along the DNA molecule and free diffusions in the nucleus.

3. Diffusion on a crowded membrane and intracellular trafficking

The organization of a cellular membrane is the determinant of the efficiency of trafficking molecules (e.g., receptors) to their destination. After decades of intense research on membrane organization, it was demonstrated recently by single-particle imaging that the effective diffusion constant can span a large spectrum of values, from 0.001 to 0.2 $\mu m^2\, s^{-1}$ (Choquet 2010), yet it is still unclear how the heterogeneity of the membrane controls diffusion (see figure 9). There are several studied examples, where changing the arrangement of absorbing windows affects the cell function. In bacteria, receptors re-cluster, depending on the external concentration of a chemotactic attractant, thus improving the sensitivity. In the context of neuroscience, receptors are known to re-cluster before the tip of a growing neuron (growth cone) turns toward a chemoattractant. Changing the arrangement of AMPA receptors in neuronal synapses affects the synaptic transmission. The variations in the shape of dendritic spines of neurons (Segal and Andersen 2000) as a result of learning and other physiological activities changes both the density and distribution of receptors, transporters and other regulatory proteins and thereby change the ionic flux through the membrane (Bourne and Harris 2008). Recently, using single molecule tracking, the diffusion coefficient of a molecule freely diffusing on intact and treated neuronal membranes, cleared of almost all obstacles, was calculated in (Renner *et al* 2009). The degree of crowding of a membrane with obstacles can be estimated from diffusion data and from an appropriate model and its analysis, as explained below. The key to assessing the crowding is to estimate the local diffusion coefficient from the measured molecular trajectories and from the analytical formula for the MFPT through a narrow passage between obstacles.

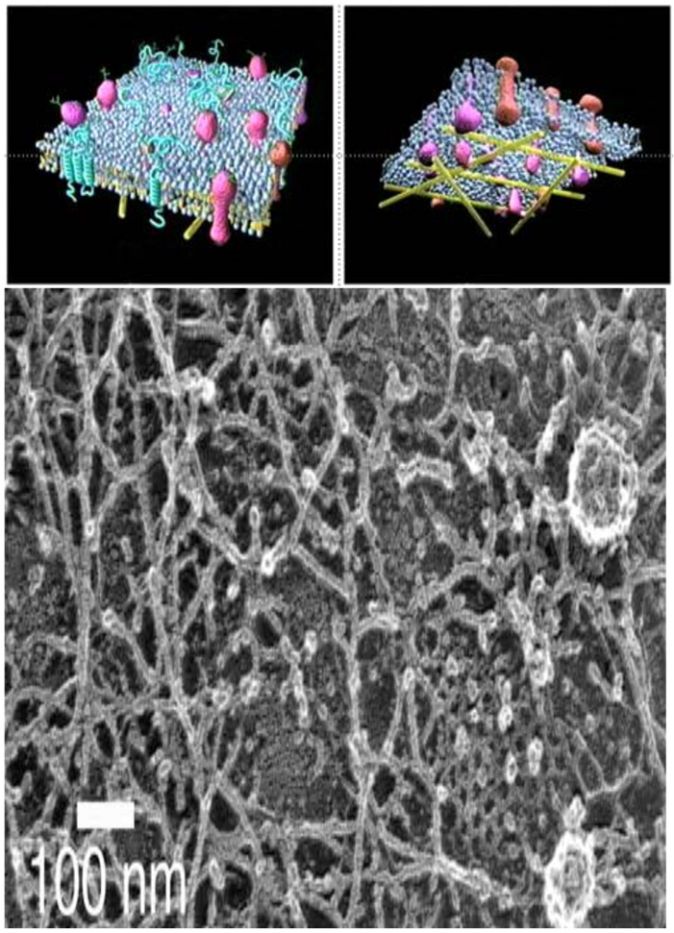

Figure 9. Organization of a neuronal membrane (www.nanobio.frontier.kyoto-u.ac.jp/lab/slides/4/e.html, reproduced with permission from A Kusumi, Copyright 2005) containing microdomains made of overlapping filaments.

3.1. Diffusion on a membrane crowded with obstacles

In a simplified model of crowding, the circular obstacles are as shown in figure 10(*a*). It is a square lattice of circular obstacles of radius a centered at the corners of lattice squares of side L. The mean exit time from a lattice box (see figure 10(*a*)) is to leading order

$$\bar{\tau}_4 = \frac{\bar{\tau}}{4}, \tag{3.1}$$

where $\bar{\tau}$ is the MFPT to a single absorbing window in narrow straits with the other windows closed (reflecting instead of absorbing) (see figure 20 (left); $\bar{\tau}$ is the MFPT from the head to the segment $\boldsymbol{AB}$, or figure 24 (left)). It follows that the waiting time in the cell enclosed by the obstacles is approximately exponentially distributed (1.1) with rate

$$\lambda = \frac{2}{\bar{\tau}_4}, \tag{3.2}$$

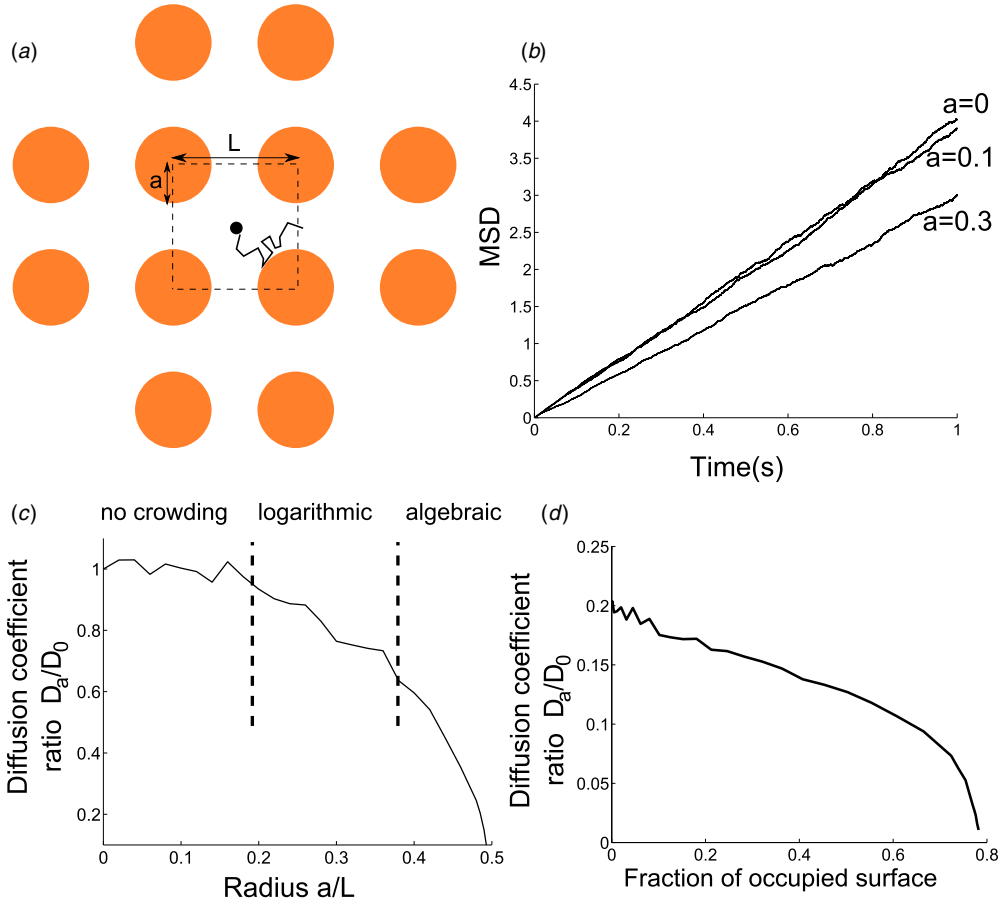

Figure 10. Model of diffusion on a crowded membrane. (*a*) Schematic representation of a Brownian particle diffusing in a crowded microdomain. (*b*) Mean square displacement (MSD) of the particle in a domain paved with microdomains. The MSD is linear, showing that crowding does not affect the nature of diffusion. The effective diffusion coefficient is computed from $\langle \mathrm{MSD}(t)/4t \rangle$. (*c*) Effective diffusion coefficient computed from the MSD for different radiuses of the obstacles. Brownian simulations (continuous curve): there are three regions (separated by the dashed lines). While there is no crowding for $a < 0.2$, the decreasing of the effective diffusion coefficient for $0.2 < a < 0.4$ is logarithmic, and like square root for $a > 0.4$. (*d*) Effective diffusion coefficient of a particle diffusing in a domain as a function of the fraction of the occupied surface. An AMPAR has a diffusion coefficient of $0.2\,\mu\mathrm{m}^2\,\mathrm{s}^{-1}$ in a free membrane.

where $\bar{\tau}$ is given by

$$\bar{\tau} \approx \begin{cases} c_1 & \text{for } 0.8 < \varepsilon < 1, \\ c_2|\Omega| \log \dfrac{1}{\varepsilon} + d_1 & \text{for } 0.55 < \varepsilon < 0.8, \\ c_3 \dfrac{|\Omega|}{\sqrt{\varepsilon}} + d_2 & \text{for } \varepsilon < 0.55, \end{cases} \tag{3.3}$$

with $\varepsilon = (L - 2a)/a$ and $d_1, d_2 = O(1)$ for $\varepsilon \ll 1$ (see figure 10). The constants c_i, $(i = 1, 2, 3)$ are calculated in Holcman *et al* (2011): the MFPT c_1 from the center to

the boundary of an unrestricted square is the solution of (6.6), given by

$$u(x,y)=\frac{4L^2}{\pi^3 D}\sum_0^\infty \frac{\left[\cosh\left(k+\frac{1}{2}\right)\pi-\cosh(k+\frac{1}{2})\pi\,(2y/L-1)\right]\sin(2k+1)\pi x/L}{(2k+1)^3\cosh(2k+1)\pi},$$

so $c_1 = u(L/2, L/2) \approx [4L^2/\pi^3 D][\cosh(\pi/2-1)/\cosh\pi]$ remains unchanged and with $L=1, D=1$, the value $c_1 \approx 0.076$ is obtained. Similarly, $c_2 = 1/2\pi D \approx 0.16$. The coefficient c_3 is approximated by $c_3 \approx \pi/8D \approx 0.39$. The coefficients d_i are chosen by patching $\bar{\tau}$ continuously between the different regimes. They are given by

$$d_1 = c_1 + c_2|\Omega(r_1)|\log(1-2r_1)$$
$$d_2 = c_1 - c_2[|\Omega(r_1)|\log(1-2r_1)+|\Omega(r_2)|\log(1-2r_2)] - c_3|\Omega(r_2)|r_2^{1/2}(1-2r_2)^{-1/2},$$

where $|\Omega(r)| = L^2 - \pi r^2$. Equation (3.3) holds in the full range of values of $a \in [0, L/2]$ and L.

Brownian simulations, with diffusion coefficient D_0, of the passage from one square to the other with fixed L and variable a (see figure 10(*b*)) confirm that in the given geometry the mean square displacement (MSD) is linear in time, so that crowding does not affect the effectively diffusive character of the Brownian motion on a sufficiently coarse time scale. The simulations also confirm that the effective diffusion coefficient can be computed from $D_a = \mathrm{MSD}(t)/4t$ for sufficiently large t. Figure 10(*c*) shows the diffusion coefficient ratio D_a/D_0 as a function of a/L. For $a = 0.3$, the value $D_a/D_0 \approx 0.7$ is obtained, whereas a direct computation with the mean exit time formula (3.3) gives

$$\frac{\tau_0}{\tau_a} = \frac{c_1}{c_2|\Omega|\log\dfrac{1}{\varepsilon}+d_1} \approx 0.69, \tag{3.4}$$

where $\varepsilon = (L-2a)/L = 0.4$. It follows that the coarse-grained diffusion coefficient is classical and the effective diffusion coefficient $D_a/D_0 = \tau_0/\tau_a$ decreases nonlinearly as a function of the radius a, as given by the uniform formula (3.3). The three regimes of equation (3.3) are recovered (figure 10(*c*)): a non-crowded regime for $a < 0.2L$, where the effective diffusion coefficient does not show any significant decrease, a region $0.2L < a < 0.4L$, where the leading order term of the effective diffusion coefficient is logarithmic, and for $a > 0.4L$ the effective diffusion coefficient decays as $\sqrt{(L-2a)/L}$, in agreement with (3.3). Thus the analytical expression for the NET through the narrow neck between obstacles coarse-grains Brownian motion in an environment crowded with obstacles (figure 10) into a Markovian random walk that jumps between the connected domains at exponentially distributed times with rates determined by the NET. This random walk can in turn be approximated by an effective coarse-grained isotropic diffusion, as done for atomic migration in crystals (Schuss 1980, chapter 8, section 2) and for effective diffusion on a surface with obstacles (Holcman *et al* 2011). The diffusion approximation to the transition probability density function of an isotropic random walk that jumps at exponentially distributed waiting times with rate λ on a square lattice with step size L is given by

$$\frac{\partial p}{\partial t} = \bar{D}\left(\frac{\partial^2 p}{\partial x^2}+\frac{\partial^2 p}{\partial y^2}\right), \quad \bar{D}=\frac{\lambda L^2}{4}. \tag{3.5}$$

To illustrate this theory, a reduction of the effective diffusion coefficient from 0.01 on a clear membrane to 0.2 $\mu\mathrm{m}^2\,\mathrm{s}^{-1}$ on an obstructed membrane (Triller and Choquet 2003), which leads to the estimate of 70% occupancy of the membrane surface with obstacles (Holcman *et al* 2011), as can be seen from figure 10.

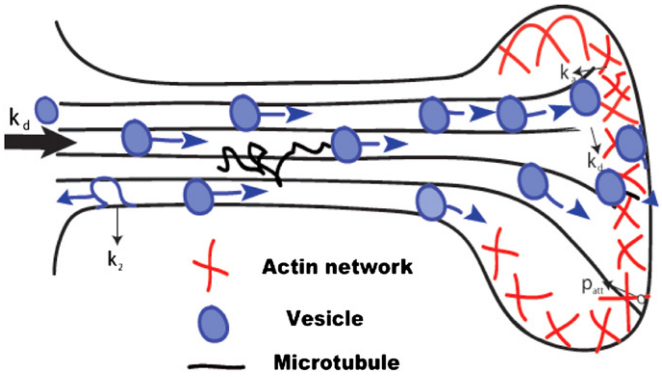

Figure 11. Schematic representation of neurite outgrowth: vesicles are delivered to the neurite tip while microtubules can associate in a bundle. When the microtubule bundle is attached to the neurite tip, the entire neurite structure is stabilized. Such a model accounts for the different between dendritic versus axonal growth (Tsaneva *et al* 2009). Reproduced with permission from Tsaneva *et al* 2009 *Biophys. J.* **96** 840–57. Copyright (2009) Elsevier.

3.2. Trafficking and the delivery flux of vesicles in neurite outgrowth

Vesicular delivery is a fundamental process of development, which requires both membrane expansion by exocytosis and cytoskeletal dynamics (Kandel *et al* 2000). It is also involved in constitutive material delivery (figure 11). To study the specific contribution of these processes and to account for live imaging data, a biophysical model was used in Tsaneva *et al* (2009) to relate the overall neurite outgrowth rate to the rate of vesicle delivery at the growth-cone tip. The vesicle motion was modeled as isotropic diffusion in a spherical domain of radius R with constant radial potential $U(\boldsymbol{x}) = -\boldsymbol{v}(\boldsymbol{x}) \cdot \boldsymbol{x}$, where $\boldsymbol{v}(\boldsymbol{x})$ is the constant field of radial average motion away from the center.

This model represents the motion of vesicles in the cell soma by a combination of Brownian motion and directed motion along microtubules (MTs) and actin filaments. The MFPT to a small neurite initiation site of radius a on the membrane was shown to be given in the large-force limit by

$$\bar{\tau} = \frac{|S|}{a|\boldsymbol{v}|}\left[1 + O\left(\frac{D}{|\boldsymbol{v}|R}\right)\right], \tag{3.6}$$

where $|S|$ is the surface area of the soma. Formula (3.6) reveals that due to the sequestration at the surface by the strong drift, the search time for Brownian motion in this case depends on the surface area of the boundary. Simulations show that Brownian trajectories stay close to the boundary surface in their search for the absorbing window (Tsaneva *et al* 2009).

3.3. References to section 3

The organization of a cellular membrane was studied in Edidin *et al* (1991), Sheetz (1993), Suzuki and Sheetz (2001), Kusumi *et al* (2005, 1993), Saxton (1995), Saxton and Jacobson (2010), Eisinger *et al* (1986), and more. Single-particle imaging results were reported in Borgdorff and Choquet (2002), Tardin *et al* (2003), Triller and Choquet (2003), Choquet (2010). It was shown in Kim *et al* (2002) that in bacteria, receptors re-cluster depending on the external concentration of a chemotactic attractant. The papers (Bouzigues *et al* 2007, 2010)

show that receptors are known to re-cluster before the tip of a growing neuron. Taflia and Holcman (2011) and Freche *et al* (2011) show that rearrangement of AMPA receptors affects synaptic transmission. Segal and Andersen (2000) report variations in the shape of dendritic spines of neurons as a result of learning and other physiological activities in changing both the density and distribution of receptors, transporters, and other regulatory proteins. Changes in ionic flux through the membrane as the result of rearrangements are reported in Bourne and Harris (2008).

4. Physical virology: modeling the early steps of cell viral infection at the molecular level

The goal of this section is to present modeling for quantifying the early steps of cell viral infection.

4.1. The cytoplasmic viral trafficking

Most viruses entering cells after binding to specific membrane receptors (Whittaker *et al* 2000, Greber and Way 2006) are enveloped in an endosomal compartment (figure 12). To undergo cytoplasmic or nuclear replication and to avoid degradation in acidic lysosomes, viruses must then successfully escape the endosome. Thus the Brownian motion of the virus can be terminated by killing the trajectory (see section 4.2.1 below). Enveloped viruses, such as influenza, contain membrane-associated glycoproteins, which mediate the fusion between the viral and endosomal membranes. In particular, acidification of the endosome triggers the conformational change of the influenza hemagglutinins (HA) into a fusogenic state, leading to endosome-virus membranes fusion and release of genes into the cytoplasm. Other non-enveloped viruses, such as the Adeno-Associated-Virus, have to escape the endosome, a process that requires one of the (less than 10) capsid proteins to change conformation. Following the endosomal escape, viruses have to travel through the crowded cytoplasm to reach the nucleus and deliver their genetic material through the nuclear pores. While the cytoplasmic movement of viral particles towards the nucleus is facilitated by the microtubular network and viral proteins, very little is known about the fate of non-viral DNA vectors in the cytoplasm. However, trapping of large DNA particles ($>$500 kDa) in the crowded cytoplasm drastically hinders their cytoplasmic diffusion (Verkman 2000, Dauty and Verkman 2005) and subsequently diminishes the transfection rate of synthetic gene vectors (see figure 13). Mathematical and physical models of this process are constructed for the purpose of predicting and quantifying infectivity and the success of gene delivery. The models give rise to rational Brownian dynamics simulations for the study of sensitivity to parameters and, eventually, for testing the increase or the drop in infectivity by using simultaneously a combination of various drugs. The modeling approach can be used for the optimization of the delivery in a high-dimensional parameter space.

For example, fusogenic peptides derived from viral glycoproteins, are increasingly used in cationic synthetic vectors and the pH-sensitivity of fusogenic glycoproteins can now be tuned by modifying the electrostatic stability of the fusogenic complex. These engineered glycoproteins are intended for designing efficient gene vectors, so quantitative models can help optimizing glycoprotein molecular properties with respect to the endosomal escape efficacy of the vector.

4.2. Stochastic description of viral trajectories

Vesicular and viral motions alternate intermittently between periods of free diffusion and directed motion along MTs. Such viral trajectories have been recently monitored by using

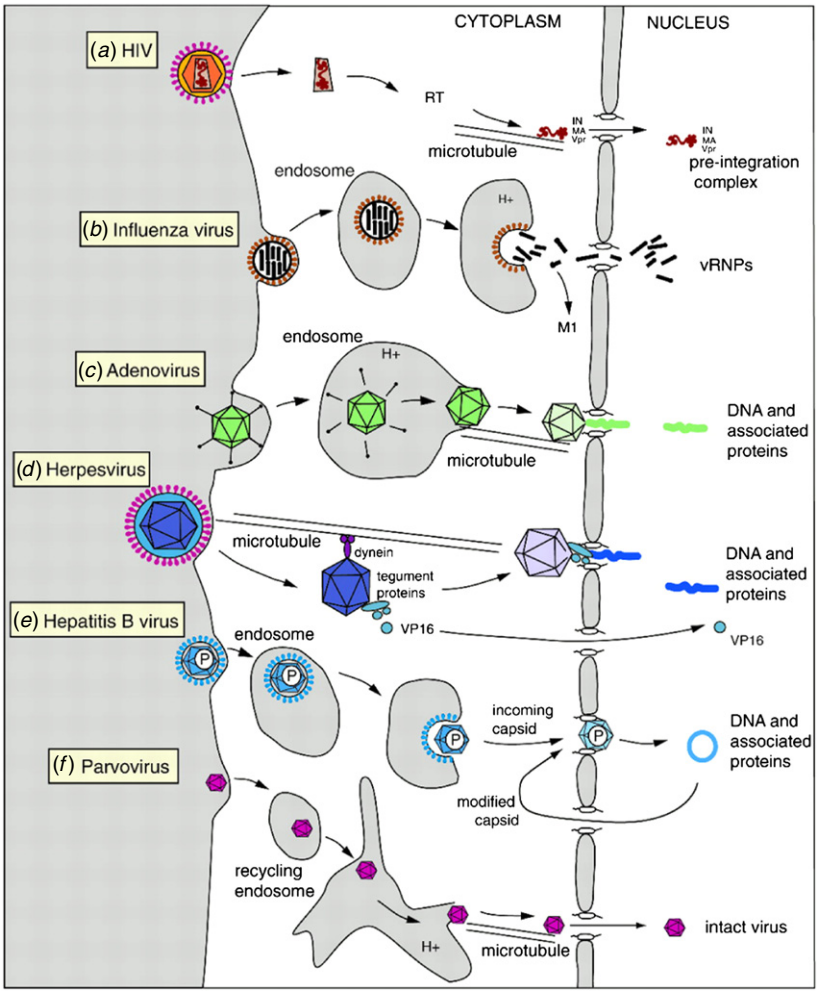

Figure 12. Common entry and uncoating mechanisms of selected nuclear-replicating viruses. Viruses can undergo substantial uncoating in the cytoplasm before translocating into the nucleus; (a) HIV, (b) influenza virus. Alternatively, viruses can dock to the NPC and uncoat at the cytoplasmic side of the nuclear membrane; (c) adenovirus and (d) herpesvirus. They may possibly disassemble within the nuclear pore; (e) hepatitis B virus; (f) parvovirus Whittaker *et al* (2000). Reproduced with permission from Whittaker *et al* 2000 *Annu. Rev. Cell Dev. Biol.* **16** 627–51. Copyright (2003) Annual Reviews.

new imaging techniques *in vivo*. The trajectory of a viral particle $\boldsymbol{x}(t)$ can be modeled as the randomly switching process

$$\mathrm{d}\boldsymbol{x}(t) = \begin{cases} \sqrt{2D}\,\mathrm{d}\boldsymbol{w} & \text{for } \boldsymbol{x}(t) \text{ free} \\ \boldsymbol{V}\,\mathrm{d}t & \text{for } \boldsymbol{x}(t) \text{ bound to a MT,} \end{cases} \tag{4.1}$$

where $\boldsymbol{w}(t)$ is standard Brownian motion, D is the diffusion constant, and $\boldsymbol{V}(\boldsymbol{x})$ is the velocity field of the directed motion along MTs.

The particle motion (4.1) can be coarse-grained by the stochastic equation

$$\mathrm{d}\boldsymbol{x} = \boldsymbol{b}(\boldsymbol{x})\,\mathrm{d}t + \sqrt{2D}\,\mathrm{d}\boldsymbol{w}, \tag{4.2}$$

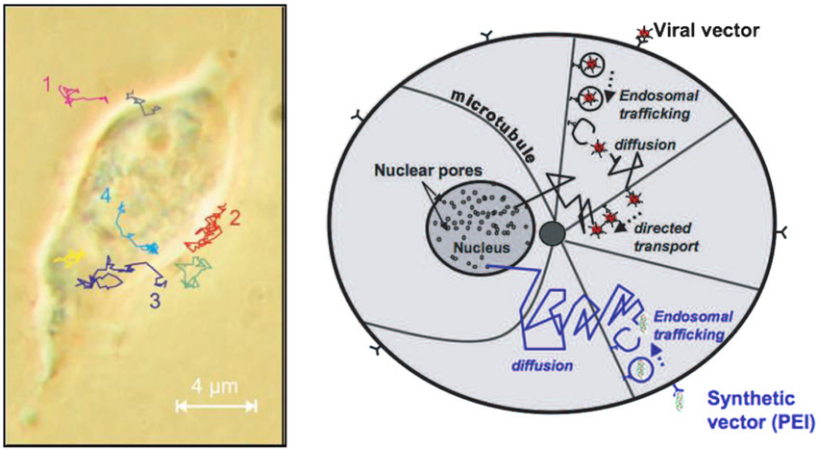

Figure 13. Virus infection in cell. (*a*) Trajectories of single AAV-Cy5 particles: the traces showing single diffusing virus particles were recorded at different times. They describe various stages of AAV infection, e.g. diffusion in solution (1 and 2), touching at the cell membrane (2), penetration of the cell membrane (3), diffusion in the cytoplasm (3 and 4), penetration of the nuclear envelope (4), and diffusion in the nucleoplasm (Seisenberger *et al* 2001). Reproduced with permission from Seisenberger *et al* 2001 *Science* **294** 1929–32. Copyright (2001) The American Association for the Advancement of Science. (*b*) Schematic description of early steps of infection for viral and synthetic vectors. Synthetic vectors are not assisted by active transport during their cytoplasmic trafficking.

where $\boldsymbol{b}(\boldsymbol{x})$ is a drift that accounts for ballistic periods along MTs. The stochastic dynamics (4.2) can be used to generate computer simulations of trajectories in free and confined environment (Schuss 2010b). It can also be used to derive asymptotic formulas for the probability and the MFPT of the virus to a nuclear pore (Holcman 2007). Various analytic expressions for the effective drift have been derived for various geometries. The expression for $\boldsymbol{b}(\boldsymbol{x})$ depends on the MT organization and on the viral dynamical properties, such as the diffusion constant D, affinity with MTs, and net velocity along MTs.

4.2.1. NET with killing. Consider the diffusion process $\boldsymbol{x}(t)$ defined by the stochastic dynamics in a domain Ω

$$\mathrm{d}\boldsymbol{x} = \boldsymbol{a}(\boldsymbol{x})\,\mathrm{d}t + \sqrt{2}\boldsymbol{B}(\boldsymbol{x})\,\mathrm{d}\boldsymbol{w}(t), \tag{4.3}$$

where $\boldsymbol{a}(\boldsymbol{x})$ is a smooth drift vector, $\boldsymbol{B}(\boldsymbol{x})$ is a diffusion tensor, and $\boldsymbol{w}(t)$ is a vector of independent standard Brownian motions. If the trajectories $\boldsymbol{x}(t)$ can be terminated at time t at each point $\boldsymbol{x} \in \Omega$ with probability $k(\boldsymbol{x}, t)\,\Delta t + o(\Delta t)$, the function $k(\boldsymbol{x}, t)$ is called killing measure (Schuss 2010b). When the boundary $\partial\Omega$ admits no absorption flux, except for a small absorbing window $\partial\Omega_a$, the NET problem is to find the absorption flux of trajectories that survive the killing. Thus there are two random termination times defined on the trajectories $\boldsymbol{x}(t)$, the time T to termination by killing and the time τ to termination by absorption in $\partial\Omega_a$.

4.2.2. The probability of absorbed trajectories. The transition probability density function of the process $\boldsymbol{x}(t)$ with killing and absorption is the conditional transition probability density

function of trajectories that have neither been killed nor absorbed in $\partial\Omega_a$ by time t,

$$p(\boldsymbol{x}, t \,|\, \boldsymbol{y})\, \mathrm{d}\boldsymbol{x} = \Pr\{\boldsymbol{x}(t) \in \boldsymbol{x} + \mathrm{d}\boldsymbol{x}, T > t, \tau > t \,|\, \boldsymbol{y}\}. \tag{4.4}$$

It is the solution of the Fokker–Planck equation (Schuss 2010b)

$$\frac{\partial p(\boldsymbol{x}, t \,|\, \boldsymbol{y})}{\partial t} = \mathcal{L}_{\boldsymbol{x}} p(\boldsymbol{x}, t \,|\, \boldsymbol{y}) - k(\boldsymbol{x}) p(\boldsymbol{x}, t \,|\, \boldsymbol{y}) \quad \text{for } \boldsymbol{x}, \boldsymbol{y} \in \Omega, \tag{4.5}$$

where $\mathcal{L}_{\boldsymbol{x}}$ is the forward operator

$$\mathcal{L}_{\boldsymbol{x}} p(\boldsymbol{x}, t \,|\, \boldsymbol{y}) = \sum_{i,j=1}^{d} \frac{\partial^2 \sigma^{i,j}(\boldsymbol{x}) p(\boldsymbol{x}, t \,|\, \boldsymbol{y})}{\partial x^i \partial x^j} - \sum_{i=1}^{d} \frac{\partial a^i(\boldsymbol{x}) p(\boldsymbol{x}, t \,|\, \boldsymbol{y})}{\partial x^i}, \tag{4.6}$$

and $\boldsymbol{\sigma}(\boldsymbol{x}) = \frac{1}{2}\boldsymbol{B}(\boldsymbol{x})\boldsymbol{B}^T(\boldsymbol{x})$. The operator $\mathcal{L}_{\boldsymbol{x}}$ can be written in the divergence form $\mathcal{L}_{\boldsymbol{x}} p(\boldsymbol{x}, t \,|\, \boldsymbol{y}) = -\nabla \cdot \boldsymbol{J}(\boldsymbol{x}, t \,|\, \boldsymbol{y})$, where the flux density vector $\boldsymbol{J}(\boldsymbol{x}, t \,|\, \boldsymbol{y})$ is

$$J^i(\boldsymbol{x}, t \,|\, \boldsymbol{y}) = -\sum_{j=1}^{d} \frac{\partial \sigma^{i,j}(\boldsymbol{x}) p(\boldsymbol{x}, t \,|\, \boldsymbol{y})}{\partial x^i} + a^i(\boldsymbol{x}) p(\boldsymbol{x}, t \,|\, \boldsymbol{y}). \tag{4.7}$$

The initial and boundary conditions for the Fokker–Planck equation (4.5) are

$$p(\boldsymbol{x}, 0 \,|\, \boldsymbol{y}) = \delta(\boldsymbol{x} - \boldsymbol{y}) \quad \text{for } \boldsymbol{x}, \boldsymbol{y} \in \Omega \tag{4.8}$$

$$p(\boldsymbol{x}, t \,|\, \boldsymbol{y}) = 0 \quad \text{for } t > 0, \quad \boldsymbol{x} \in \partial\Omega_a, \ \boldsymbol{y} \in \Omega \tag{4.9}$$

$$\boldsymbol{J}(\boldsymbol{x}, t \,|\, \boldsymbol{y}) \cdot \boldsymbol{n}(\boldsymbol{x}) = 0 \quad \text{for } t > 0, \quad \boldsymbol{x} \in \partial\Omega - \partial\Omega_a, \ \boldsymbol{y} \in \Omega. \tag{4.10}$$

The probability that the particle reaches the absorbing $\partial\Omega_a$ before being killed is given by Holcman *et al* (2005b) and Schuss (2010b)

$$\Pr\{T < \tau \,|\, \boldsymbol{y}\} = \int_0^\infty \int_\Omega k(\boldsymbol{x}) p(\boldsymbol{x}, t \,|\, \boldsymbol{y})\, \mathrm{d}\boldsymbol{x}\, \mathrm{d}t. \tag{4.11}$$

The absorption probability flux on $\partial\Omega_A$ is $J(t \,|\, \boldsymbol{y}) = \oint_{\partial\Omega} \boldsymbol{J}(\boldsymbol{x}, t \,|\, \boldsymbol{y}) \cdot \boldsymbol{n}(\boldsymbol{x})\, \mathrm{d}S_{\boldsymbol{x}}$ and $\int_0^\infty J(t \,|\, \boldsymbol{y})\, \mathrm{d}t$ is the probability of trajectories that have ever been absorbed at $\partial\Omega_a$.

The probability distribution function of the killing time T is the conditional probability of killing before time t of trajectories that have not been absorbed in $\partial\Omega_a$ by that time,

$$\Pr\{T < t \,|\, \tau > t, y\} = \frac{\Pr\{T < t, \tau > t \,|\, \boldsymbol{y}\}}{\Pr\{\tau > t \,|\, \boldsymbol{y}\}} = \frac{\int_0^t \int_\Omega k(\boldsymbol{x}) p(\boldsymbol{x}, s \,|\, \boldsymbol{y})\, \mathrm{d}\boldsymbol{x}\, \mathrm{d}s}{\int_0^\infty \int_\Omega k(\boldsymbol{x}) p(\boldsymbol{x}, s \,|\, \boldsymbol{y})\, \mathrm{d}\boldsymbol{x}\, \mathrm{d}s}.$$

The probability distribution of the time to absorption at $\partial\Omega_a$ is the conditional probability of absorption before time t of trajectories that have not been killed by that time,

$$\Pr\{T < t \,|\, \tau > t, y\} = \frac{\int_0^t J(s \,|\, \boldsymbol{y})\, \mathrm{d}s}{1 - \int_0^\infty \int_\Omega k(\boldsymbol{x}) p(\boldsymbol{x}, s \,|\, \boldsymbol{y})\, \mathrm{d}\boldsymbol{x}\, \mathrm{d}s}. \tag{4.12}$$

Thus the NET is the conditional expectation of the absorption time of trajectories that are not killed in Ω, that is,

$$\mathbb{E}[\tau \,|\, T > \tau, \boldsymbol{y}] = \int_0^\infty \Pr\{\tau > t \,|\, T > \tau, \boldsymbol{y}\}\, \mathrm{d}t = \frac{\int_0^\infty s J(s \,|\, \boldsymbol{y})\, \mathrm{d}s}{1 - \int_0^\infty \int_\Omega k(\boldsymbol{x}) p(\boldsymbol{x}, s \,|\, \boldsymbol{y})\, \mathrm{d}\boldsymbol{x}\, \mathrm{d}s}.$$

The survival probability of trajectories that have not been terminated by time t is given by

$$S(t \,|\, \boldsymbol{y}) = \int_\Omega p(\boldsymbol{x}, t \,|\, \boldsymbol{y})\, \mathrm{d}\boldsymbol{x}. \tag{4.13}$$

The mean time spent at $\boldsymbol{x}$ prior to termination,

$$\tilde{p}(\boldsymbol{x} \,|\, \boldsymbol{y}) = \int_0^\infty p(\boldsymbol{x}, t \,|\, \boldsymbol{y})\, \mathrm{d}t \tag{4.14}$$

is the solution of the boundary value problem

$$\begin{aligned}
&\mathcal{L}_x\tilde{p}(\boldsymbol{x}\,|\,\boldsymbol{y}) - k(\boldsymbol{x})\tilde{p}(\boldsymbol{x}\,|\,\boldsymbol{y}) = -\delta(\boldsymbol{x}-\boldsymbol{y}) \quad \text{for } \boldsymbol{x},\boldsymbol{y}\in\Omega\\
&\tilde{p}(\boldsymbol{x}\,|\,\boldsymbol{y}) = 0 \quad \text{for } \boldsymbol{x}\in\partial\Omega_a,\ \boldsymbol{y}\in\Omega\\
&\boldsymbol{J}(\boldsymbol{x}\,|\,\boldsymbol{y})\cdot\boldsymbol{n}(\boldsymbol{x}) = 0 \quad \text{for } t>0,\ \boldsymbol{x}\in\partial\Omega-\partial\Omega_a,\ \boldsymbol{y}\in\Omega.
\end{aligned} \tag{4.15}$$

If the initial pdf is a sufficiently smooth function $p_I(\boldsymbol{x})$, the density of the time spent at $\boldsymbol{x}$ prior to termination,

$$\tilde{p}(\boldsymbol{x}) = \int_\Omega \tilde{p}(\boldsymbol{x}\,|\,\boldsymbol{y})p_I(\boldsymbol{y})\,\mathrm{d}\boldsymbol{y}, \tag{4.16}$$

satisfies

$$\begin{aligned}
&\mathcal{L}_x\tilde{p}(\boldsymbol{x}) - k(\boldsymbol{x})\tilde{p}(\boldsymbol{x}) = -p_I(\boldsymbol{x}) \quad \text{for } \boldsymbol{x}\in\Omega\\
&\tilde{p}(\boldsymbol{x}) = 0 \quad \text{for } \boldsymbol{x}\in\partial\Omega_a\\
&\tilde{\boldsymbol{J}}(\boldsymbol{x})\cdot\boldsymbol{n}(\boldsymbol{x}) = 0 \quad \text{for } t>0,\ \boldsymbol{x}\in\partial\Omega-\partial\Omega_a.
\end{aligned} \tag{4.17}$$

The probability P_N of trajectories that start at $\boldsymbol{y}\in\Omega$ and are terminated at $\partial\Omega_a$ is

$$P_N = \int_\Omega \Pr\{\tau\langle T\,|\,\boldsymbol{x}(0)=\boldsymbol{y}\}p_I(\boldsymbol{y})\,\mathrm{d}\boldsymbol{y} = 1 - \int_\Omega k(\boldsymbol{x})\tilde{p}(\boldsymbol{x})\,\mathrm{d}\boldsymbol{x}. \tag{4.18}$$

4.3. Probability that a viral particle arrives alive at a nuclear pore

For Brownian motion with diffusion coefficient 1 (without drift) the boundary value problem (4.17) can be solved asymptotically for a small absorbing window $\partial\Omega_a$ in terms of the Neumann function $N(\boldsymbol{x},\boldsymbol{\xi})$, which is a solution of the boundary value problem

$$\begin{aligned}
&\Delta_x N(\boldsymbol{x},\boldsymbol{\xi}) = -\delta(\boldsymbol{x}-\boldsymbol{\xi}) \quad \text{for } \boldsymbol{x},\boldsymbol{\xi}\in\Omega,\\
&\frac{\partial N(\boldsymbol{x},\boldsymbol{\xi})}{\partial n(\boldsymbol{x})} = -\frac{1}{|\partial\Omega|} \quad \text{for } \boldsymbol{x}\in\partial\Omega,\boldsymbol{\xi}\in\Omega,
\end{aligned} \tag{4.19}$$

and is defined up to an additive constant. Multiplying (4.17) by $N(\boldsymbol{x},\boldsymbol{\xi})$ and using Green's theorem, the identity

$$\tilde{p}(\boldsymbol{\xi}) = -\int_\Omega N(\boldsymbol{x},\boldsymbol{\xi})[-p_I(\boldsymbol{x}) + k(\boldsymbol{x})\tilde{p}(\boldsymbol{x})]\mathrm{d}\boldsymbol{x} + \int_{\partial\Omega_a} N(\boldsymbol{x},\boldsymbol{\xi})\frac{\partial\tilde{p}(\boldsymbol{x})}{\partial n}\,\mathrm{d}S_x + \frac{1}{|\partial\Omega|}\int_{\partial\Omega}\tilde{p}(\boldsymbol{x})\,\mathrm{d}S_x$$

is obtained. The leading order term in the expansion of $\tilde{p}(\boldsymbol{x})$ for small $|\partial\Omega_a|$ and sufficiently small killing rate $k(\boldsymbol{x},t)$ (i.e., smaller than the absorption rate, see Holcman (2007)) is constant $\tilde{p}(\boldsymbol{x})\approx P_a$ outside a boundary layer near $\partial\Omega_a$. Then the following approximation is valid,

$$\tilde{p}(\boldsymbol{\xi}) \approx \int_{\partial\Omega_a} N(\boldsymbol{x},\boldsymbol{\xi})\frac{\partial\tilde{p}(\boldsymbol{x})}{\partial n}\,\mathrm{d}S_x + P_a\left(1 - \int_\Omega k(\boldsymbol{x})N(\boldsymbol{x},\boldsymbol{\xi})\,\mathrm{d}\boldsymbol{x}\right) + \int_\Omega N(\boldsymbol{x},\boldsymbol{\xi})p_I(\boldsymbol{x})\,\mathrm{d}\boldsymbol{x}.$$

The compatibility condition, obtained from the integration of (4.17) over Ω, and the boundary layer expansion (see Holcman (2007)), give in the three-dimensional case the approximation of the density of the time spent at $\boldsymbol{x}\in\Omega$ as

$$P_a \approx \frac{1}{4\varepsilon + \int_\Omega k(\boldsymbol{x})\,\mathrm{d}\boldsymbol{x}}, \tag{4.20}$$

provided (see Schuss 2013 and Holcman and Schuss 2014)

$$\frac{|\partial\Omega|^{1/(d-1)}}{|\Omega|^{1/d}} = O(1) \quad \text{for } \varepsilon \ll 1, \tag{4.21}$$

and the probability of the absorbed trajectories as

$$P_N = 1 - \int_\Omega k(\boldsymbol{x})\tilde{p}(\boldsymbol{x})\,\mathrm{d}\boldsymbol{x} \approx \frac{4\varepsilon}{4\varepsilon + \int_\Omega k(\boldsymbol{x})\,\mathrm{d}\boldsymbol{x}} \quad \text{for } k(\boldsymbol{x}) \ll 1. \tag{4.22}$$

If the diffusion coefficient is D, the parameter ε in (4.20) and (4.22) is changed to $D\varepsilon$. The case of Brownian motion with drift is described in Holcman (2007). The results of this section are used to estimate the probability that a live virus arrives at one of the small pores in a cell's nucleus.

4.4. The mean arrival time to a small nuclear pore

The crowded cytoplasm is a risky environment for gene vectors that can be either trapped or degraded through the cellular defense machinery. Thus cytoplasmic trafficking is rate-limiting and to analyze quantitatively that step, asymptotic expressions for the probability P_N and the mean arrival time $\mathbb{E}\tau$ of a virus vector to one of n small nuclear pores $\partial\Omega_a$ were derived in Holcman (2007) and Lagache *et al* (2009b).

Viral degradation or immobilization is modeled as a steady state degradation rate $k(\boldsymbol{x})$. The probability density function $p(\boldsymbol{x}, t)$ of viral trajectories that survive by time t in the cytoplasm Ω is defined as the joint probability and density of the trajectory, the killing time T, and the time to absorption τ,

$$p(\boldsymbol{x}, t)\,\mathrm{d}\boldsymbol{x} = \Pr\{\boldsymbol{x}(t) \in \boldsymbol{x} + \mathrm{d}\boldsymbol{x}, T > t, \tau > t\} \tag{4.23}$$

with initial viral pdf $p_I(\boldsymbol{x})$. The probability P_N of trajectories that start with the viral pdf in Ω and are terminated at $\partial\Omega_a$ is calculated from the expression for the NET as follows. For n identical nuclear pores in the shape of absorbing disks of radius ε and when $\boldsymbol{b}(\boldsymbol{x}) = -\nabla\Phi(\boldsymbol{x})$ for some potential $\Phi(\boldsymbol{x})$, the leading order terms in the expansions of P_N and $\mathbb{E}\tau$ for small ε are given by Amoruso *et al* (2011) as

$$P_N \approx \frac{\frac{1}{|\partial\Omega|}\oint_{\partial\Omega} \exp\left\{-\frac{\Phi(\boldsymbol{x})}{D}\right\}\mathrm{d}\boldsymbol{x}}{\frac{1}{|\partial D|}\oint_{\partial D} \exp\left\{-\frac{\Phi(\boldsymbol{x})}{D}\right\}\mathrm{d}\boldsymbol{x} + \left(\frac{1}{4nD\varepsilon} + \frac{1}{DC_\Omega}\right)\int_\Omega k(\boldsymbol{x}) \exp\left\{-\frac{\Phi(\boldsymbol{x})}{D}\right\}\mathrm{d}\boldsymbol{x}}$$

and

$$\mathbb{E}\tau \approx \frac{\left(\frac{1}{4nD\varepsilon} + \frac{1}{DC_\Omega}\right)\int_\Omega \exp\left\{-\frac{\Phi(\boldsymbol{x})}{Dcal}\right\}\mathrm{d}\boldsymbol{x}}{\frac{1}{|\partial D|}\oint_{\partial D} \exp\left\{-\frac{\Phi(\boldsymbol{x})}{D}\right\}\mathrm{d}\boldsymbol{x} + \left(\frac{1}{4nD\varepsilon} + \frac{1}{DC_\Omega}\right)\int_\Omega k(\boldsymbol{x}) \exp\left\{-\frac{\Phi(\boldsymbol{x})}{D}\right\}\mathrm{d}\boldsymbol{x}},$$

where C_Ω is the capacity of the nucleus (for a sphere of radius δ, $C_\Omega = 4\pi\delta$). Interestingly, for a biological cell with a spherical nucleus (radius $\delta = 5\,\mu$m), the $n = 2000$ circular nuclear pores (radius $\varepsilon = 25$ nm) cover a surface $n\pi\varepsilon^2/4\pi\delta^2 \approx 1\%$ of the total nuclear surface and $1/4nD\varepsilon$ is only one third of $1/C_\Omega$.

4.5. Endosomal viral escape

Once a virus enters an endosome, it has to escape into the cytoplasm before being degraded by lysosomes. Although the exact pathways leading to endosomal escape are not fully elucidated, they are limiting steps. Most viruses possess efficient endosomolytic proteins allowing them to disrupt the endosomal membrane, such as the VP1 penetration protein of the adeno-associated virus or the influenza HA. In addition, the biophysical mechanism leading to endosomal membrane destabilization and concomitant plasmids release for synthetic vectors is still poorly understood. However, in both cases, acidification of the endosome is needed to trigger endosomal escape. For viruses, protons or low pH-activated proteases bind viral endosomolytic proteins, triggering their conformational change into a fusogenic state. The

case of proton-binding sites on the viral envelope of the influenza virus has also been discussed (see references below).

Models aimed at estimating the residence time of a viral particle inside an endosomal compartment are based on the assessment of the accumulation of discrete proton-binding events, that lead to the conformational change of HAs. These models, for both enveloped and non-enveloped viruses, consist of two steps. In the first step, the concentration of protons is fixed and the mean time for protons to bind to fundamental protein binding sites until a threshold is reached is calculated from a jump-Markov-process model by asymptotic methods. A conformational change into a fusogenic state is triggered after the threshold is reached. In the second step, the dynamics of endosomal escape is modeled by coupling the pH-dependent conformational change of glycoproteins with the proton-influx rate. The impact of the size of the endosome on the escape kinetics and pH can be mathematically predicted. It reconciles different experimental observations: while a virus can escape from small endosomes (radius of 80 nm) in the cell periphery at pH $\sim$ 6 in about 10 min, it can also be routed towards the nuclear periphery, where escape from larger endosomes (radius of 400 nm) is rapid (less than 1 min) at pH $=$ 5. The detailed modeling of these two steps were reviewed in Amoruso *et al* (2011).

4.6. References to section 4

Mathematical and physical models of the viral infection process were proposed in Holcman (2007), Lagache and Holcman (2008a, 2008b), Amoruso *et al* (2011), Lagache *et al* (2009a). Optimization of the virus delivery in a high-dimensional parameter space is discussed in Lagache *et al* (2012). Synthetic vectors are discussed in Abe *et al* (1998) and Tu and Kim (2008). Tuning of the pH-sensitivity of fusogenic glycoproteins is discussed in Rachakonda *et al* (2007). Escape efficacy of the vector is discussed in Sodeik (2000).

Vesicular and viral motions that alternate intermittently between periods of free diffusion and directed motion along MTs are discussed in Greber and Way (2006). Such viral trajectories have been recently monitored by using new imaging techniques *in vivo* (Seisenberger *et al* 2001, Brandenburg and Zhuang 2007).

The MFPT of a virus to a nuclear pore was calculated in Holcman (2007). The effective drifts of viral motion have been derived for various geometries in Lagache and Holcman (2008a, 2008b).

The adeno-associated virus and the influenza HA have been discussed in Farr *et al* (2005) and Huang *et al* (2002). Models aimed at estimating the residence time of a viral particle inside an endosomal compartment are considered in Lagache *et al* (2012). The key to the calculation of the MFPT of the Markovian jump process model is the method of Knessl *et al* (1984a), Matkowsky *et al* (1984) and Knessl *et al* (1984b). The detailed modeling of two key steps in the viral release was reviewed in Amoruso *et al* (2011).

5. The NET in neurobiology and synaptic transmission

As mentioned above, the NET reflects the role of the cell's geometrical structure in determining the cell's biological function. Next, illustrations are given of the way the NET is manifested in modeling synaptic transmission and in the simulation, analysis, and interpretation of the output of the models. The explicit asymptotic formulas for the NET also coarse-grain spatial organization of a fundamental domain, called the PSD, which is discussed in detail below.

To address the structure-function question in molecular-level cell models, the discussion is focused on the regulation of diffusion flux in synapses and dendritic spines of neurons, whose

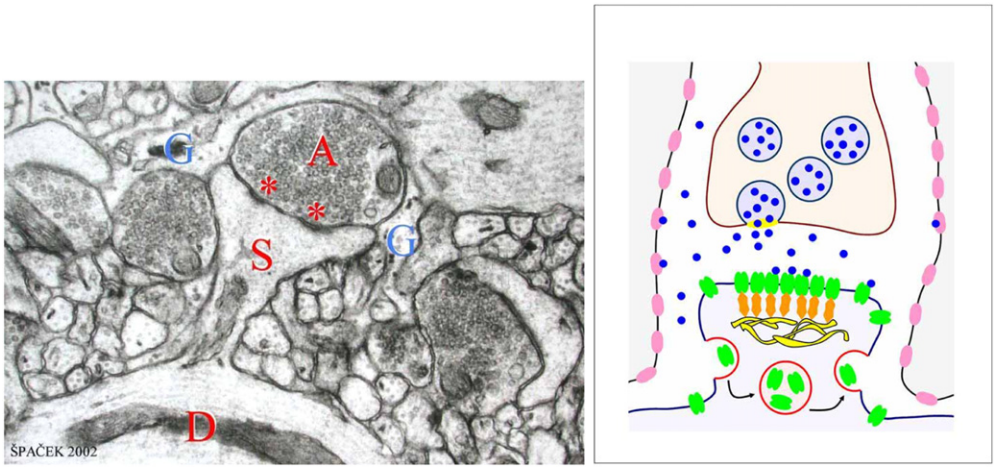

Figure 14. A neuronal synapse. Left panel: electron microscopy of a synapse. The post-synaptic terminal is located on a dendritic spine (S) branched in the dendrite (D). The glial cells (G) are located around the axon (A). (Spacek J 2002). Reproduced with permission from Spacek J 2002 *Psychiatrie*, Suppl. 3 **6** 55–60. Copyright (2002) Tigis. Right panel: schematic representation of a synapse between neurons. Neurotransmitters (blue) are released to the synaptic cleft at the presynaptic terminal and can find a receptor (green) on the post-synaptic terminal or be absorbed by the surrounding glial cells (red). The post-synaptic density (PSD) is the dense region above the yellow sheet holding the scaffolding molecules (orange).

spatial structure has been studied extensively (see list of references below). A schematic representation of a synapse between neurons is given in figure 14.[3] By its very definition, synapses are local active micro-contacts underlying direct neuronal communication but depending on the brain area where they are located and their specificity, they can vary in size and molecular composition. The molecular processes underlying synaptic transmission are well known: after NTs such as glutamate, released from a vesicle located on the surface of a pre-synaptic neuron (see figure 14), they diffuse inside the synaptic cleft, composed of pre- and post-synaptic terminals. The post-synaptic terminal of an excitatory synapse contains ionotropic glutamate receptors such as AMPA and NMDA and they may open upon binding to NTs. When NTs diffuse in the cleft, they can either find a specific receptor protein on the membrane of the post-synaptic terminal, such as NMDA, AMPA, and so on[4], or are absorbed by the surrounding glia cells and recycled. Relevant terminology, illustrations, and movies for the biological material can be found in Wikipedia. More generally, there are various types of synapses characterized by the NT molecules, such as the small molecules acetylcholine (ACh), dopamine (DA), norepinephrine (NE), serotonin (5-HT), histamine, epinephrine, or the amino acids gamma-aminobutyric acid (GABA), glycine, glutamate, aspartate, and many others[5] that are released at the presynaptic terminal into the flat cylindrically-shaped synaptic cleft when an action potential (signal) reaches the presynaptic terminal. Once a receptor binds a ligand NT molecule (or molecules) it opens to the passage of ions, which diffuse in the cleft from the pre- to the post-synaptic terminal (also called neuronal spine), thus transmitting the signal

[3] This lower figure is based on www.niaaa.nih.gov/Resources/GraphicsGallery/Neuroscience/Pages/synapsebetween_neurons.aspx.

[4] see, e.g. http://en.wikipedia.org/wiki/Biochemical_receptor.

[5] see, e.g., http://en.wikipedia.org/wiki/Neurotransmitter.

across the synapse into the neuronal spine. The signal propagates in the form of a diffusion flux of ions, such as calcium or sodium, through the spine neck into the dendrite (see idealized mathematical models of spine structure in figure 20).

For example, AMPA receptors are tetrameric assemblies composed of four different subunits, which can bind to a glutamate molecule. However, two glutamate molecules are required to open a single AMPA channel. The amplitude of ionic current is thus proportional to the number of open receptors and their conductances. The post-synaptic current measures the efficiency of synaptic transmission and is related to the frequency and location of released vesicles in a complex manner (see list of references below).

This section reviews some properties of synaptic transmission based on a diffusion model in microdomains. The presented methods serve to estimate the mean and the variance of the post-synaptic current. Indeed, this current plays a fundamental role in neuronal communication: it is the direct and fast signal of synaptic transmission. It activates the post-synaptic neuron or modulates its membrane potential. This current not only depends on receptors such as AMPA, but also on the complex molecular machinery edifice underneath that controls them. Possible changes in the current dynamics is the readout of synaptic plasticity, a process that underlies learning and memory.

The transmitted diffusion flux can be regulated by the number and distribution of the receptors, by the length of the spine neck, the number and distribution of ionic channels and pumps on the spine neck that can leak ions from the neck, and many other structural factors. Mathematical models of synapse components provide much information about their function (see section 5.3 below).

5.1. A model of the synaptic current

A general approach to the estimation of the synaptic current is proposed next. The diffusion of glutamate molecules in the cleft geometry, which is approximated by a flat cylinder, is described by a direct analysis of AMPA conductances rather than by the classical Markov description, obtained by optimal fitting of measurements performed outside a synapse. The presented method accounts for the four glutamate binding sites per receptor. While glutamate molecules are Brownian inside the cylindrical synaptic cleft Ω, AMPARs are positioned on the PSD (see figures 14 (right) and 16 (right)). The model of glutamate binding to an AMPAR is a radiative boundary condition on the PSD ($\Omega_{\rm PSD}$), as described below.

When a glutamate molecule hits the lateral boundary ($\partial\Omega_{\rm Lat}$) of the cleft (modeled as a cylinder Ω), it is absorbed and no longer can contribute to the activation of AMPARs. The pdf $p(\boldsymbol{x}, t|\boldsymbol{x}_0)$ of a Brownian glutamate molecule $\boldsymbol{x}(t)$, given $\boldsymbol{x}(0) = \boldsymbol{x}_0 \in \Omega$, is the solution of the initial-boundary value problem for the diffusion equation

$$\frac{\partial p(\boldsymbol{x}, t|\boldsymbol{x}_0)}{\partial t} = D\Delta p(\boldsymbol{x}, t|\boldsymbol{x}_0) \quad \text{for } \boldsymbol{x} \in \Omega,\ t > 0 \tag{5.1}$$

$$\begin{aligned} &p(\boldsymbol{x}, 0) = \delta(\boldsymbol{x} - \boldsymbol{x}_0) \quad \text{for } \boldsymbol{x} \in \Omega \\ &\frac{\partial p(\boldsymbol{x}, t|\boldsymbol{x}_0)}{\partial \nu} = 0 \quad \text{for } \boldsymbol{x} \in \partial\Omega_r \\ &p(\boldsymbol{x}, t|\boldsymbol{x}_0) = 0 \quad \text{for } \boldsymbol{x} \in \partial\Omega_{\rm Lat} \\ &-D\frac{\partial p(\boldsymbol{x}, t|\boldsymbol{x}_0)}{\partial \nu} = -\kappa\, p(\boldsymbol{x}, t|\boldsymbol{x}_0) \quad \text{for } \boldsymbol{x} \in \partial\Omega_{\rm PSD}, \end{aligned} \tag{5.2}$$

where D is diffusion constant of a free glutamate molecule. The partial absorption rate constant κ not only accounts for the fraction of AMPARs inside the PSD, but also for the activation

barrier of a single glutamate to a glutamate receptor binding site. The rate constant

$$\kappa = \frac{D}{2\pi R_{\mathrm{PSD}}^2} \frac{1}{\frac{1}{N_a a} + \frac{D}{\kappa_e 2\pi a^2 N_a}} \tag{5.3}$$

was proposed in Taflia and Holcman (2011), where a and R_{PSD} are the radii of a single receptor and the PSD, respectively, and N_a is the number of AMPARs. This rate constant was derived in (appendix of Taflia and Holcman 2011) by considering that the N_a receptors are placed on the PSD which has a surface πR_{PSD}^2. The criterion is that the flux to all receptors is equal to the flux with the partial absorbing constant κ. Here D is the diffusion constant of glutamate molecules in the cleft and κ_e is the partial reflecting rate constant generated by a single AMPAR on a glutamate molecule. This constant is calibrated from (patch-clamp) experimental data.

The probability $p(\boldsymbol{x}_0)$ that a glutamate molecule binds a receptor released at $\boldsymbol{x}_0$, is the total probability flux into the receptors, that is, into the absorbing boundary $\partial\Omega_{\mathrm{PSD}}$,

$$p(\boldsymbol{x}_0) = D \int_0^\infty \int_{\partial\Omega_{\mathrm{PSD}}} \frac{\partial p(\boldsymbol{y}, t \,|\, \boldsymbol{x}_0)}{\partial n} \,\mathrm{d}\boldsymbol{y}\,\mathrm{d}t = D \int_{\partial\Omega_{\mathrm{PSD}}} \frac{\partial u(\boldsymbol{y} \,|\, \boldsymbol{x}_0)}{\partial n} \,\mathrm{d}\boldsymbol{y}, \tag{5.4}$$

where $u(\boldsymbol{x} \,|\, \boldsymbol{x}_0) = \int_0^\infty p(\boldsymbol{x}, t \,|\, \boldsymbol{x}_0)\,\mathrm{d}t$ satisfies

$$\begin{aligned}
&D\Delta u(\boldsymbol{x} \,|\, \boldsymbol{x}_0) = -\delta(\boldsymbol{x} - \boldsymbol{x}_0) \quad \text{for } \boldsymbol{x} \in \Omega \\
&\frac{\partial u(\boldsymbol{x} \,|\, \boldsymbol{x}_0)}{\partial \nu} = 0 \quad \text{for } \boldsymbol{x} \in \partial\Omega_r \\
&u(\boldsymbol{x} \,|\, \boldsymbol{x}_0) = 0 \quad \text{for } \boldsymbol{x} \in \partial\Omega_{\mathrm{Lat}} \\
&D\frac{\partial u(\boldsymbol{x} \,|\, \boldsymbol{x}_0)}{\partial \nu} = \kappa u(\boldsymbol{x} \,|\, \boldsymbol{x}_0) \quad \text{for } \boldsymbol{x} \in \partial\Omega_{\mathrm{PSD}}.
\end{aligned} \tag{5.5}$$

Brownian trajectories that are absorbed in a small receptor are rare and can hardly be expected to provide sufficient statistical data for a reliable estimate of the number of saturated receptors. It is necessary, therefore, to coarse-grain the simulation by deriving analytical approximations to $u(\boldsymbol{x} \,|\, \boldsymbol{x}_0)$ and $p(\boldsymbol{x}_0)$, to be used in numerical simulations. The absorbing rate constant κ_e in equation (5.3) is obtained by calibrating with the experimental value $\kappa_e \approx 1.6$ (see Taflia and Holcman 2011).

5.2. The mean and variance of the synaptic current I_s

To compute the mean and the variance of the synaptic current the number of bound glutamate molecules and the probability of a given configuration of bound AMPARs have to be accounted for. To estimate the first, recall that the probability distribution $\mathrm{Pr}_k(\boldsymbol{x}_0)$ of k independent bound glutamate molecules, after a vesicle is released at $\boldsymbol{x}_0$, follows the binomial distribution

$$\mathrm{Pr}_k(\boldsymbol{x}_0) = C_{4N_a}^k p(\boldsymbol{x}_0)^k (1 - p(\boldsymbol{x}_0))^{4N_a - k}, \tag{5.6}$$

where N_a is the mean number of bound glutamates and $p(\boldsymbol{x}_0)$ is the probability that a glutamate binds one of the receptors before it escapes. It is given by equation (5.4), as

$$p(\boldsymbol{x}_0) = \kappa \int_{\partial\Omega_{\mathrm{PSD}}} u(\boldsymbol{x} \,|\, \boldsymbol{x}_0)\,\mathrm{d}S(\boldsymbol{x}). \tag{5.7}$$

The mean and the variance of the number of bound receptors are given by $M(\boldsymbol{x}_0) = N_g p(\boldsymbol{x}_0)$ and $\sigma^2(\boldsymbol{x}_0) = N_g p(\boldsymbol{x}_0)(1 - p(\boldsymbol{x}_0))$, respectively. When the vesicle is released at the center of the synapse, for a PSD and a synaptic radius of respectively 300 nm and 500 nm (the effective surface area of a single AMPAR is $10\,\mathrm{nm}^2$ and $\kappa = 0.25$ see figure 15), the probability $p(\boldsymbol{x}_0) = 8.10^{-3}$ for a glutamate molecule to hit a cluster of AMPARs is found in Taflia and Holcman (2011).

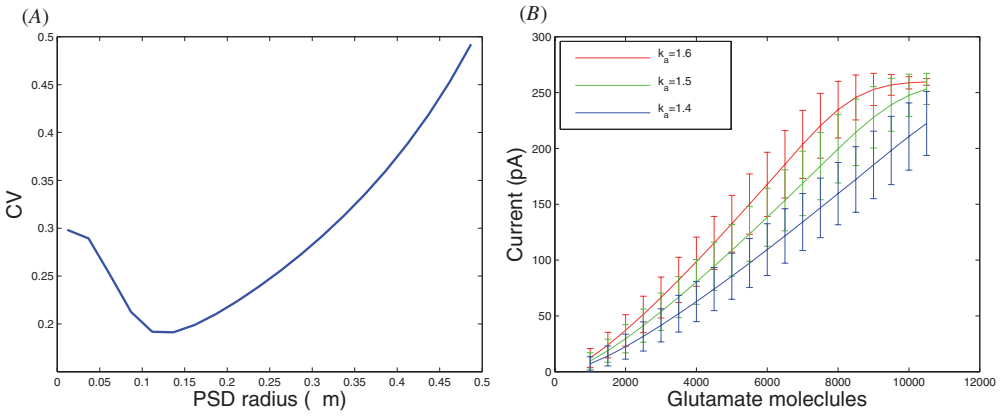

Figure 15. (*A*) The coefficient of variation (CV) reaches a maximum for a PSD of radius of 0.3 μm. This shows that for a given size of the active zone, where vesicles are released, the CV is minimum when receptors are spread over an optimal PSD area. (*B*) Calibration of the partial absorption rate constant κ. The synaptic current is simulated according to (5.9) for different values of the activation coefficient κ (see (5.3)). The optimal synaptic response in the range of 3000–12000 glutamate molecules is achieved at $\kappa = 1.6$.

An additional source of fluctuations in the number of bound AMPARs is as follows. AMPARs can bind from zero to four glutamate molecules. Therefore the probability $\Pr\{\vec{n}\,|\,k\}$ of a given configuration $\vec{n} = (n_4, n_3, n_2, n_1)$ of n_1 AMPARs that bind one glutamate molecule, n_2 AMPARs that bind 2, and so on, when there are N_a AMPA receptors and $k < 4N_a$ bound glutamate molecules, is given by

$$\Pr\{\vec{n}\,|\,k\} = \frac{N_a!}{n_4!n_3!n_2!n_1!(N_a - (n_4+n_3+n_2+n_1))!}\,\frac{1}{F(k,N_a)}. \tag{5.8}$$

This is the probability of choosing at random n_4 AMPARs out of N_4, n_3 out of $N_a - n_4$, and so on. $F(k, N_a)$ is the total number of possibilities to decompose the number k as a sum of N_a summands from the set of integers $\{4, 3, 2, 1, 0\}$. The number $F(k, N_a)$ can be computed numerically as the $(k+1)$th coefficient in the expansion of $(1+x+x^2+x^3+x^4)^{N_a}$ in powers of x. With the notation V for the potential and $\vec{\gamma} = (\gamma_1, \gamma_2, \gamma_3, \gamma_4)$ for the conductance vector, given these probabilities, all moments of the current can be found, and in particular, the mean and variance are given by

$$\begin{aligned}
\langle I_s(\boldsymbol{x}_0)\rangle &= \sum_{k=1}^{N_g}\sum_{n\in S_k} \vec{n}\cdot\vec{\gamma}\,\Pr\{\vec{n}\,|\,k\}V\Pr_k(\boldsymbol{x}_0)\\
&= \sum_{k=1}^{4N_a}\sum_{n\in S_k} \vec{n}\cdot\vec{\gamma}\,\Pr\{\vec{n}\,|\,k\}\Pr_k(\boldsymbol{x}_0)V + N_a\gamma_4 V\left(1-\sum_{k=0}^{4N_a}\Pr_k(\boldsymbol{x}_0)\right)\\
\langle I_s^2(\boldsymbol{x}_0)\rangle &= \sum_{k=1}^{N_g}\sum_{n\in S_k} (\vec{n}\cdot\vec{\gamma})^2\,\Pr\{\vec{n}\,|\,k\}\Pr_k(\boldsymbol{x}_0)V^2 - \langle I_s(\boldsymbol{x}_0)\rangle^2\sum_{k=1}^{4N_a}\sum_{n\in S_k}(\vec{n}\cdot\vec{\gamma}V)^2\,\Pr\{\vec{n}\,|\,k\}\Pr_k(\boldsymbol{x}_0)\\
&\quad + (N_a\gamma_4 V)^2\left(1-\sum_{k=0}^{4N_a}\Pr_k(\boldsymbol{x}_0)\right) - \langle I_s(\boldsymbol{x}_0)\rangle^2.
\end{aligned} \tag{5.9}$$

Here S_k is the set of all the possible configurations of $\vec{n} = (n_1, n_2, n_3, n_4)$ such that $4n_4 + 3n_3 + 2n_2 + n_1 = k$. The formulae for the mean and variance are composed of two terms: in the first one, the summation extends over sites that do not bind the maximal number of glutamate molecules. The probability for such an event is the product of the probabilities $\Pr_k$, that k glutamates are bound ($k < 4N_a$) and the probability $\Pr\{\vec{n}\,|\,k\}$ for a given binding configuration $k = 4n_4 + 3n_3 + 2n_2 + n_1$. The second term accounts for the event where all AMPAR binding sites are occupied ($4N_a$), the probability is the complementary to the one associated with the partial binding of the first case. Figure 15(*A*) shows that the coefficient of variation (CV = SD/Mean, where SD stands for standard deviation) has a minimum as a function of the size of the PSD. This unexpected result is further discussed in Taflia and Holcman (2011).

5.3. Leakage in a conductor of Brownian particles

A conductor of Brownian particles is a bounded domain Ω, with a source of particles on the boundary or in the interior and a target, which is an absorbing part $\partial\Omega_a$ of $\partial\Omega$. The remaining boundary $\partial\Omega_r$ is reflecting. Some of the Brownian particles may leak out of Ω not through $\partial\Omega_a$ if $\partial\Omega_r$ contains a small absorbing hole $S(\varepsilon)$. The calculation of the leakage flux is not the same as that in the narrow escape problem, because the boundary flux does not vanish as the small hole shrinks. The leakage problem is to find the flux through the small hole $S(\varepsilon)$.

The (dimensionless) stationary density $u(\boldsymbol{x})$ of the Brownian particles satisfies the mixed boundary value problem

$$\begin{aligned} &D\Delta u(\boldsymbol{x}) = 0 \quad \text{for } \boldsymbol{x} \in \Omega \\ &\frac{\partial u(\boldsymbol{x})}{\partial \nu} = 0 \quad \text{for } \boldsymbol{x} \in \partial\Omega_r \\ &-D\frac{\partial u(\boldsymbol{x})}{\partial \nu} = \phi(\boldsymbol{x}) \quad \text{for } \boldsymbol{x} \in \partial\Omega_s \\ &u(\boldsymbol{x}) = 0 \quad \text{for } \boldsymbol{x} \in \partial\Omega_a \cup S(\varepsilon). \end{aligned} \tag{5.10}$$

The leakage flux,

$$J_\varepsilon = D\int_{S(\varepsilon)} \frac{\partial u(\boldsymbol{x})}{\partial \nu}\, \mathrm{d}S_{\boldsymbol{x}}, \tag{5.11}$$

is given in terms of the solution $u_0(\boldsymbol{x})$ of the reduced problem (without the leak $S(\varepsilon)$). The leakage flux J_ε can be found by determining the flux of each eigenfunction and then by using eigenfunction expansion. The eigenvalue problem for (5.10) is

$$-D\Delta u_\varepsilon(\boldsymbol{x}) = \lambda(\varepsilon)u_\varepsilon(\boldsymbol{x}) \quad \text{for } \boldsymbol{x} \in \Omega \tag{5.12}$$

$$\frac{\partial u_\varepsilon(\boldsymbol{x})}{\partial \nu} = 0 \quad \text{for } \boldsymbol{x} \in \partial\Omega_s \cup \partial\Omega_r \tag{5.13}$$

$$u_\varepsilon(\boldsymbol{x}) = 0 \quad \text{for } \boldsymbol{x} \in S(\varepsilon) \cup \partial\Omega_a. \tag{5.14}$$

The eigenvalues have a regular expansion

$$\lambda(\varepsilon) = \lambda(0) + \lambda_1\varepsilon + o(\varepsilon), \tag{5.15}$$

where $\lambda(0)$ is the eigenvalue of the reduced problem. The reduced Green function is the solution of the mixed boundary value problem with $D = 1$,

$$-\Delta G(\boldsymbol{x}, \boldsymbol{y}) = \delta(\boldsymbol{x} - \boldsymbol{y}) \quad \text{for } \boldsymbol{x}, \boldsymbol{y} \in \Omega \tag{5.16}$$

$$\frac{\partial G(\boldsymbol{x}, \boldsymbol{y})}{\partial \nu} = 0 \quad \text{for } \boldsymbol{x} \in \partial\Omega_s \cup \Omega_r,\ \boldsymbol{y} \in \Omega \tag{5.17}$$

$$G(\boldsymbol{x},\boldsymbol{y}) = 0, \quad \text{for } \boldsymbol{x} \in \partial\Omega_a,\ \boldsymbol{y} \in \Omega. \tag{5.18}$$

Multiplying (5.16) by $u_\varepsilon(\boldsymbol{x})$ and integrating over Ω, we get

$$u_\varepsilon(\boldsymbol{x}) = -\lambda(\varepsilon)\int_\Omega G(\boldsymbol{x},\boldsymbol{y})u_\varepsilon(\boldsymbol{y})\,\mathrm{d}\boldsymbol{y} + \int_{S(\varepsilon)} G(\boldsymbol{x},\boldsymbol{y})\frac{\partial u_\varepsilon(\boldsymbol{y})}{\partial \nu}\,\mathrm{d}S_y. \tag{5.19}$$

In view of the boundary condition (5.14), equation (5.19) gives for all $\boldsymbol{x} \in S(\varepsilon)$

$$\lambda(\varepsilon)\int_\Omega G(\boldsymbol{x},\boldsymbol{y})u_\varepsilon(\boldsymbol{y})\,\mathrm{d}\boldsymbol{y} = \int_{S(\varepsilon)} G(\boldsymbol{x},\boldsymbol{y})\frac{\partial u_\varepsilon(\boldsymbol{y})}{\partial \nu}\,\mathrm{d}S_y. \tag{5.20}$$

The integral on the left hand side of (5.20) can be expanded about the center of $S(\varepsilon)$ in the form

$$\int_\Omega \lambda(\varepsilon)G(\boldsymbol{x},\boldsymbol{y})u_\varepsilon(\boldsymbol{y})\,\mathrm{d}\boldsymbol{y} = G_0(\varepsilon) + O(|\boldsymbol{x}|) \quad \text{for } \boldsymbol{x} \in S(\varepsilon), \tag{5.21}$$

where the origin is assumed to be at the center of $S(\varepsilon)$ and the (x_1, x_2) plane is that of $S(\varepsilon)$. Using Popov's theorem (Popov 1992, Schuss 2013, Holcman and Schuss 2014), the following two equations are obtained (Singer *et al* 2008)

$$\lambda(\varepsilon)\int_\Omega u_\varepsilon(\boldsymbol{x})\,\mathrm{d}\boldsymbol{x} = 4\varepsilon D\frac{G_0(\varepsilon) + O(\varepsilon^2\log\varepsilon)}{1 + O(\varepsilon\log\varepsilon)} + O(\varepsilon^2\log\varepsilon) + D\int_{\partial\Omega_a}\frac{\partial u_\varepsilon(\boldsymbol{y})}{\partial\nu}\,\mathrm{d}S_y$$

$$G_0(\varepsilon) = \lambda(\varepsilon)\int_\Omega G(\boldsymbol{0},\boldsymbol{y})u_\varepsilon(\boldsymbol{y})\,\mathrm{d}\boldsymbol{y}. \tag{5.22}$$

This gives

$$\lambda(\varepsilon)\int_\Omega u_\varepsilon(\boldsymbol{x})\,\mathrm{d}\boldsymbol{x} = 4\varepsilon D\frac{\lambda(\varepsilon)\int_\Omega G(\boldsymbol{0},\boldsymbol{y})u_\varepsilon(\boldsymbol{y})\,\mathrm{d}\boldsymbol{y} + O(\varepsilon^2\log\varepsilon)}{1 + O(\varepsilon\log\varepsilon)} + O(\varepsilon^2\log\varepsilon) + D\int_{\partial\Omega_a}\frac{\partial u_\varepsilon(\boldsymbol{y})}{\partial\nu}\,\mathrm{d}S_y.$$

Solving for $\lambda(\varepsilon)$ gives

$$\begin{aligned}\lambda(\varepsilon) &= \frac{D\int_{\partial\Omega_a}\frac{\partial u_\varepsilon(\boldsymbol{y})}{\partial\nu}\,\mathrm{d}S_y + O(\varepsilon^2\log\varepsilon)}{\int_\Omega u_\varepsilon(\boldsymbol{x})\,\mathrm{d}\boldsymbol{x} - \frac{4\varepsilon D}{1+O(\varepsilon\log\varepsilon)}\int_\Omega G(\boldsymbol{0},\boldsymbol{y})u_\varepsilon(\boldsymbol{y})\,\mathrm{d}\boldsymbol{y} + O(\varepsilon^2\log\varepsilon)} \\ &= \frac{D\int_{\partial\Omega_a}\frac{\partial u_\varepsilon(\boldsymbol{y})}{\partial\nu}\,\mathrm{d}S_y}{\int_\Omega u_\varepsilon(\boldsymbol{x})\,\mathrm{d}\boldsymbol{x}}\left(1 + \frac{4\varepsilon D\int_\Omega G(\boldsymbol{0},\boldsymbol{y})u_\varepsilon(\boldsymbol{y})\,\mathrm{d}\boldsymbol{y}}{\int_\Omega u_\varepsilon(\boldsymbol{x})\,\mathrm{d}\boldsymbol{x}}\right) + O(\varepsilon^2\log\varepsilon).\end{aligned} \tag{5.23}$$

Note that due to (5.15),

$$\frac{D\int_{\partial\Omega_a}\frac{\partial u_\varepsilon(\boldsymbol{y})}{\partial\nu}\,\mathrm{d}S_y}{\int_\Omega u_\varepsilon(\boldsymbol{x})\,\mathrm{d}\boldsymbol{x}} = \lambda(0) + O(\varepsilon). \tag{5.24}$$

Obviously, $u_\varepsilon \to u_0$ as $\varepsilon \to 0$, where u_0 is the corresponding eigenfunction of the reduced problem (see also Ward and Keller 1993), so

$$\begin{aligned}\lim_{\varepsilon\to 0}\int_\Omega G(\boldsymbol{x},\boldsymbol{y})u_\varepsilon(\boldsymbol{y})\,\mathrm{d}\boldsymbol{y} &= \int_\Omega G(\boldsymbol{x},\boldsymbol{y})u_0(\boldsymbol{y})\,\mathrm{d}\boldsymbol{y} \\ \lim_{\varepsilon\to 0}\int_{\partial\Omega_a}\frac{\partial u_\varepsilon(\boldsymbol{y})}{\partial\nu}\,\mathrm{d}S_y &= \int_{\partial\Omega_a}\frac{\partial u_0(\boldsymbol{y})}{\partial\nu}\,\mathrm{d}S_y.\end{aligned}$$

Therefore (5.22) gives the flux of $u_\varepsilon(\boldsymbol{x})$ through the small hole as

$$\begin{aligned}J(\varepsilon) &= D\int_{S(\varepsilon)}\frac{\partial u_\varepsilon(\boldsymbol{y})}{\partial\nu}\,\mathrm{d}S_y = 4\varepsilon\lambda(0)D\int_\Omega G(\boldsymbol{0},\boldsymbol{y})u_0(\boldsymbol{y})\,\mathrm{d}\boldsymbol{y} + O(\varepsilon^2\log\varepsilon) \\ &= 4\varepsilon D u_0(\boldsymbol{0}) + O(\varepsilon^2\log\varepsilon).\end{aligned} \tag{5.25}$$

The function $DG(\boldsymbol{x}, \boldsymbol{y})$ is Green's function for the mixed boundary value problem (5.16)–(5.18) with diffusion coefficient D, rather than 1. Finally, expanding the solution $u(\boldsymbol{x})$ of (5.10) in eigenfunctions, (5.25) gives

$$J_\varepsilon = 4\varepsilon D u_0(\mathbf{0})\,(1 + O(\varepsilon \log \varepsilon))\,, \tag{5.26}$$

where $u_0(\boldsymbol{x})$ is the solution of the reduced problem (5.10). In dimensional variables, this gives

$$J_\varepsilon = 4aDp_0(\mathbf{0}) + O\left(\frac{a^2}{|\Omega|^{2/3}} \log \frac{a}{|\Omega|^{1/3}}\right), \tag{5.27}$$

where $p_0(\mathbf{0})$ is the value of the reduced stationary density at the hole.

Remark 5.1. Note that the asymptotic formula (5.26) holds if $\varepsilon \ll L/R$, so the source is outside the boundary layer near the hole.

An alternative approach to study diffusion in narrow domains is to use the averaging methods of (Reingruber and Holcman 2011a, Taflia and Holcman 2011), where the probability of binding before exit is computed.

5.4. Regulation of flux in a neuronal spine neck and across a thin synaptic cleft

Leakage through a small hole in a cylindrical conductor of Brownian particles is manifested in two specific neuronal structures related to synaptic dynamics. One is in regulating calcium dynamics in dendritic spines, for example, by extruding calcium from exchangers embedded on the endoplasmic reticulum inside dendritic spines (see Segal and Andersen (2000), Svoboda *et al* (1996) and Bloodgood and Sabatini (2005)). The other concerns the probability of NTs released from a vesicle into the synaptic cleft to bind to small receptors on the post-synaptic membrane. This process determines the synaptic current.

In the mathematical description of the diffusion of calcium ions from the spine head to the dendrite, the spine neck is a circular cylinder of length L and radius R, whose bases S_0 and S_L are centered at the z-axis, at $z = 0$ and $z = L$, respectively, and are parallel to the (x, y) plane. The lateral surface S_r, which in general represents the internal membrane of the endoplasmic reticulum, is impermeable to Brownian trajectories (Holcman *et al* 2004). A constant net flux ϕ is injected at S_0 (see figure 16 (left)). The flux through a small absorbing circular hole $S(\varepsilon)$ of (dimensional) radius ε on the lateral surface of the cylinder is determined by the NET from the source to the hole. The following two situations are considered: (i) a given flux at S_0, absorption at S_L, and reflection at $r = R$, and (ii) a given flux at a point source at distance r from the center of S_0, reflection at S_L, and absorption at $r = R$. The model (i) can describe the diffusion flux of calcium ions through pumps in the neck of a neuronal spine, by applying (5.27). In model (ii) the NET determines the flux of NTs from a vesicle released at distance r from the center of the presynaptic membrane S_0 into the NMDA or AMPA receptor channels in the post-synaptic membrane in the synaptic cleft (see figure 16 (right)). If the point of injection $\boldsymbol{A}$ is moved r away from the center of S_0, the decay of the flux through the receptor at the center of the PSD $\boldsymbol{B}$ is given by (5.27). Here the point $\mathbf{0}$ is the center of the hole in S_L. Both problems (i) and (ii) are solved with the leakage formula (5.27).

To solve problems (i) and (ii), the variables are scaled with L, so the dimensionless polar coordinates in the cylinder are

$$0 < \zeta < 1, \quad 0 < \rho < \frac{R}{L}, \quad 0 \leqslant \theta < 2\pi\,.$$

The solution of the reduced problem (i) for the dimensionless system (5.10) with influx density $\phi(\rho, \theta)$ at $\zeta = 0$ is constructed by method of separation of variables. For a point source at the

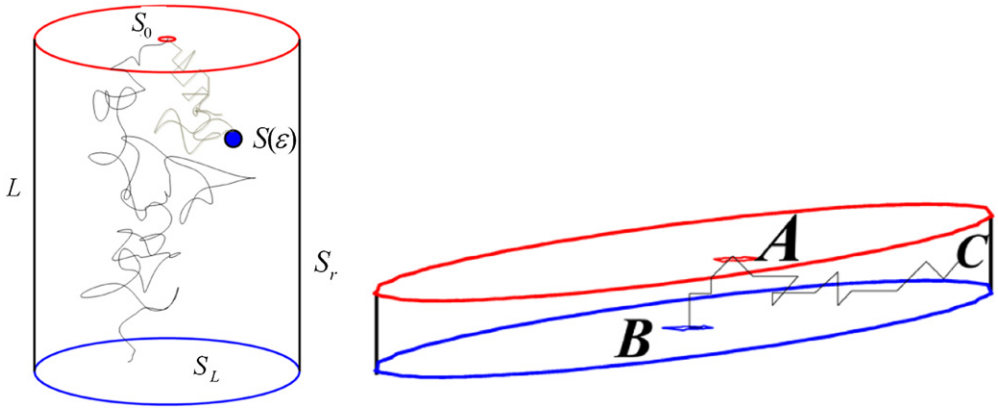

Figure 16. Left: a neck of radius R and length L. The lateral surface S_r and the upper base S_0 are reflecting, the lower base S_L and the small circular hole $S(\varepsilon)$ are absorbing. The trajectory from S_0 to $S(\varepsilon)$ is a leak trajectory. Right: an idealized model of the synaptic cleft. Neurotransmitters are injected at $\boldsymbol{A}$ and can find a receptor on the PSD $\boldsymbol{B}$ or be absorbed by the surrounding glial cells $\boldsymbol{C}$.

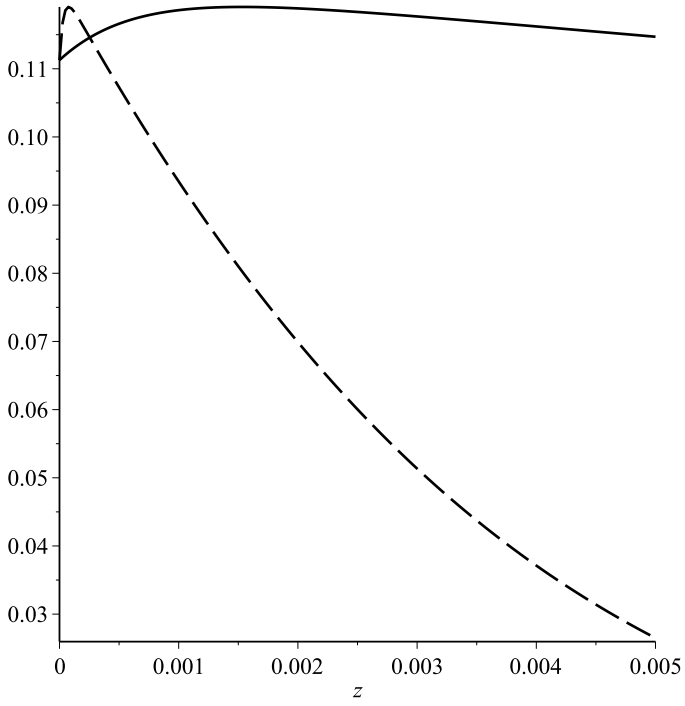

Figure 17. The exit probability $\Pr\{\tau_{\text{hole}} < \tau_{S_r}\}$ for a single pump on the neck membrane versus distance x of pump from the top, according to the separation of variables solution. Pump size is 1 nm, top curve corresponds to $L/R = 5$, and bottom curve—to $L/R = 100$.

center of S_0 the exit probability through a small hole at $r = R$ and z is shown in figure 17. If the source is uniformly distributed in S_0, the dimensionless solution of the reduced problem (i) is $u_0\,(R/L, \zeta, \theta) = C(1 - \zeta)$, where C is a constant. The dimensionless solution of the

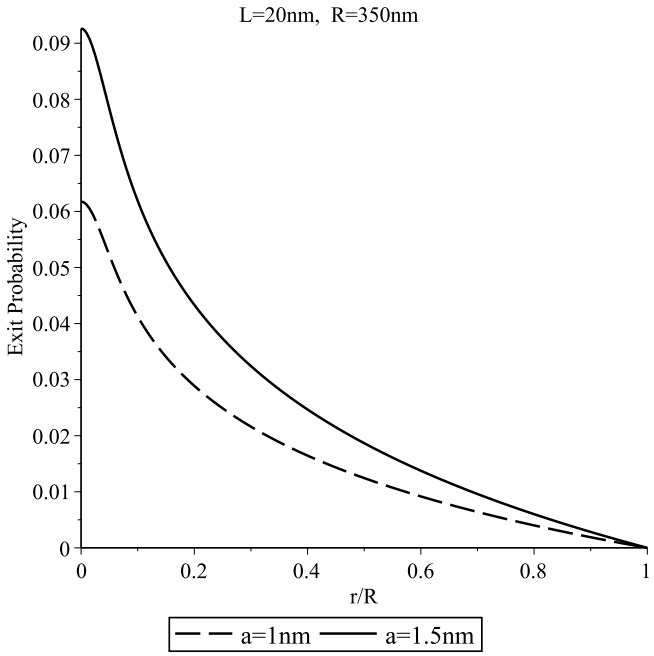

Figure 18. Binding probability $\Pr\{\tau_{\text{hole}} < \tau_{S_r}\}$ to a single AMPAR channel of radius a in a synaptic cleft of height $L = 20$ nm in a PSD of radius $R = 350$ nm versus normalized distance from center r/R, according to (5.30). Top curve: $a = 1.5$ nm, bottom curve: $a = 1$ nm.

reduced problem (ii) with influx density of a point source at $(\zeta, \rho, \theta) = (0, 0, 0)$, gives at the other end $\zeta = 1$ the density

$$u_0(\rho, 1, 0) = \sum_{m=1}^{\infty} \frac{LJ_0\left(\frac{\gamma_{0,m}L\rho}{R}\right)}{\tilde{D}\pi R\gamma_{0,m}J_0'^2(\gamma_{0,m})\sinh\frac{\gamma_{0,m}L}{R}}, \tag{5.28}$$

where $\gamma_{0,m}$ is the mth root of the Bessel function $J_0(x)$. Because the efflux through the lateral equals the influx through S_0, the probability that a Brownian particle injected at the source will reach a hole centered at $(r, L, 0)$ (in dimensional variables) is, according to the definition

$$\varepsilon = \frac{\pi|\partial\Omega_a|}{|\partial\Omega|} = \frac{\pi a}{|\partial\Omega|} \ll 1, \tag{5.29}$$

(5.26), or (5.27),

$$\Pr\{\tau_{\text{hole}} < \tau_{S_r}\} = \frac{4aL}{\pi R^2}\sum_{m=1}^{\infty}\frac{J_0\left(\frac{\gamma_{0,m}r}{R}\right)}{\gamma_{0,m}J_0'^2(\gamma_{0,m})\sinh\frac{\gamma_{0,m}L}{R}} + O\left(\frac{a^2}{R^2}\log\frac{a}{R}\right). \tag{5.30}$$

If $r = 0$, then

$$\Pr\{\tau_{\text{hole}} < \tau_{S_r}\} = \frac{4aL}{\pi R^2}\sum_{m=1}^{\infty}\frac{1}{\gamma_{0,m}J_0'^2(\gamma_{0,m})\sinh\frac{\gamma_{0,m}L}{R}} + O\left(\frac{a^2}{R^2}\log\frac{a}{R}\right).$$

The sensitivity of the flux to the location of the PSD, in the synaptic cleft is shown in figures 18 and 19 (left). The flux, averaged over a uniform distribution of the PSD is shown in figure 19 (right). The sensitivity to the height of the cleft is also shown in the figures. These sensitivities

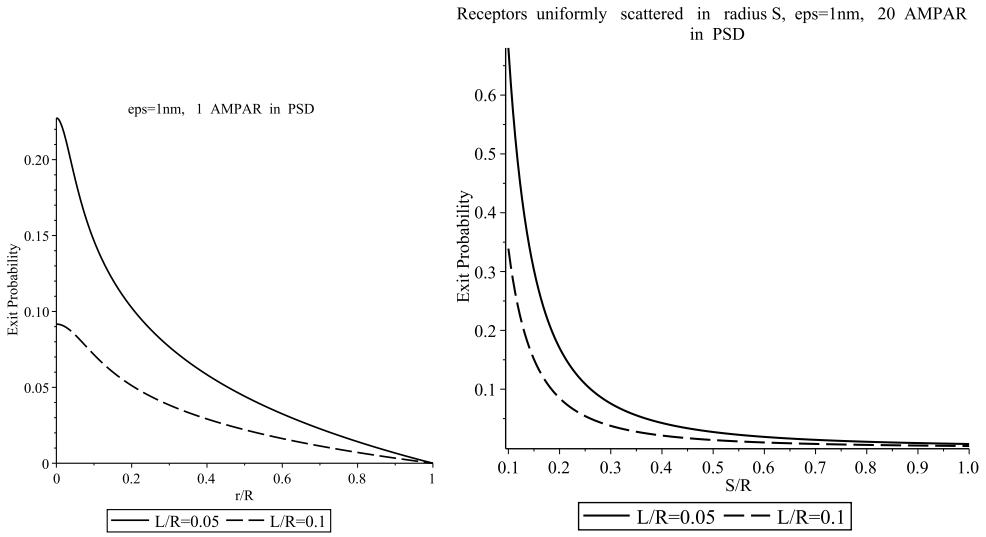

Figure 19. Left: binding probability $\Pr\{\tau_{\text{hole}} < \tau_{S_r}\}$ to an AMPA receptor in a cluster of 7 in the PSD. Right: the binding probability for 20 AMPA receptors scattered uniformly within radius $r < R$, according (5.30) averaged with respect to the uniform density. Top curve: $L/R = 0.05$, bottom curve: $L/R = 0.1$.

may hint at a possible way of regulating synaptic transmission in the cleft of a neuronal synapse by changing the location of the PSD or its size (e.g., anchoring more NMDA or AMPA receptors there). Consequently, the probability for a NT to hit the PSD remains very low and the present computation gives only an upper bound. It was found in Taflia and Holcman (2011), by using a model with a partially absorbing boundary, that the probability to bind to receptors in the PSD is of the order of 10^{-3}. This is, however, compensated by a large number of NTs, of the order of $3\ 10^3$.

5.5. References to section 5

The leakage problem of section 5.3 was solved in Singer *et al* (2008). The role of cell geometry in controlling the diffusion flux and in determining cell function, as revealed by the microscopic studies of Harris and Stevens (1988) and Bourne and Harris (2008), is elaborated in Svoboda *et al* (1996), Korkotian (2004), Hotulainen and Hoogenraad (2010) and Newpher and Ehlers (2009). It is stated in Rosenmund *et al* (1998) and Gebhardt *et al* (2006) that AMPA receptors can bind to a glutamate molecule. However, Jonas *et al* (1993) reports that two glutamate molecules are required to open a single AMPA channel. The post-synaptic current depends on the frequency and location of released vesicles (Madison *et al* 1991).

The connection of synaptic plasticity to learning and memory is related in Madison *et al* (1991). Regulation of synaptic plasticity by geometry is discussed in Korkotian (2004), Majewska *et al* (2000), Svoboda *et al* (1996), Biess *et al* (2007) and Holcman and Kupka (2010). Regulation of the number and type of receptors that contribute to the shaping of the synaptic current is discussed in Bredt and Nicoll (2003), Shi *et al* (1999), Malinow and Malenka (2002), Choquet and Borgdorff (2002), Triller and Choquet (2003), Holcman and Triller (2006) and Holcman *et al* (2005a).

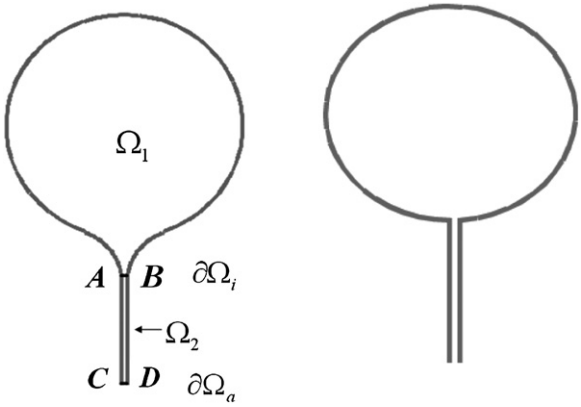

Figure 20. Mathematical idealizations of the cross sections of neuronal spine morphologies as composite domains: Left: the bulky head Ω_1 is connected smoothly by an interface $\partial\Omega_i = AB$ to a narrow neck Ω_2. The entire boundary is $\partial\Omega_r$ (reflecting), except for a small absorbing part $\partial\Omega_a = CD$. Right: the head, shown separately in figure 1, is connected to the neck without a funnel.

A general approach to the estimation of the synaptic current was developed in Taflia and Holcman (2011). A model of cleft geometry as a flat cylinder was proposed in Bourne and Harris (2008). The traditional description of AMPAR binding in terms of a Markov jump process is given in Jonas *et al* (1993). It is based on optimal fitting of measurements performed outside a synapse (Gebhardt *et al* 2006). The radiative boundary condition for binding AMPAR in the PSD was proposed in Zwanzig (1990).

6. Diffusion in composite domains

A composite domain consists of a number of bulky heads interconnected by narrow necks, such as a dumbbell-shaped domain (see figure 22). The simplest case is a planar composite domain Ω with a head Ω_1, connected through a small interface $\partial\Omega_i$ to a narrow cylindrical neck Ω_2 (figure 20 (left)). When the boundary of Ω reflects Brownian trajectories, except at the far end of Ω_2, denoted $\partial\Omega_a$, which is absorbing, the NET problem is to evaluate the MFPT from Ω_1 to $\partial\Omega_a$. In figure 20 (left) the interface $\partial\Omega_i$ is the black segment AB and the absorbing boundary $\partial\Omega_a$ is the segment CD at the bottom of the strip. The surface of revolution obtained by rotating the domain in the figure about its axis of symmetry has a similar structure. The interface $\partial\Omega_i$ in this case is a circle. Thus the length of the interface $|\partial\Omega_i|$ is given by

$$|\partial\Omega_i| = \begin{cases} a & \text{for a line segment} \\ 2\pi a & \text{for a circle.} \end{cases} \tag{6.1}$$

The following lemma is needed for the calculation of the MFPT $\bar{\tau}_{\boldsymbol{x}\to\partial\Omega_a}$.

Lemma 6.1. *The MFPT from a point $\boldsymbol{x} \in \Omega_1$ to $\partial\Omega_a$ satisfies the renewal equation*

$$\bar{\tau}_{\boldsymbol{x}\to\partial\Omega_a} = \bar{\tau}_{\boldsymbol{x}\to\partial\Omega_i} + \int_{\partial\Omega_i} G(\boldsymbol{x}\,|\,\boldsymbol{\xi})\bar{\tau}_{\boldsymbol{\xi}\to\partial\Omega_a}\,\mathrm{d}S_{\boldsymbol{\xi}}, \tag{6.2}$$

where $G(\boldsymbol{x}\,|\,\boldsymbol{\xi})$ is Green's function for the mixed boundary value problem

$$\begin{aligned} &\Delta u(\boldsymbol{x}) = 0 \quad \textit{for } \boldsymbol{x} \in \Omega_1 \\ &\frac{\partial u(\boldsymbol{x})}{\partial n} = 0 \quad \textit{for } \boldsymbol{x} \in \partial\Omega_1 - \partial\Omega_i, \quad u(\boldsymbol{x}) = \varphi(\boldsymbol{x}) \quad \textit{for } \boldsymbol{x} \in \partial\Omega_i. \end{aligned} \tag{6.3}$$

Proof. The identity follows from the fact that both sides of (6.2) satisfy (6.3) for $\boldsymbol{x} \in \Omega_1$ and coincide on $\partial\Omega_i$. □

The identity (6.2) can be interpreted as

$$\bar{\tau}_{\boldsymbol{x}\to\partial\Omega_a} = \bar{\tau}_{\boldsymbol{x}\to\partial\Omega_i} + \bar{\tau}_{\partial\Omega_i\to\partial\Omega_a}, \tag{6.4}$$

where the MFPT $\bar{\tau}_{\partial\Omega_i\to\partial\Omega_a}$ is $\bar{\tau}_{\boldsymbol{x}\to\partial\Omega_a}$, averaged over $\partial\Omega_i$ with respect to the flux density of Brownian trajectories in Ω_1 into an absorbing boundary at $\partial\Omega_i$ (see Schuss 2010b for further details).

Theorem 6.2 (The NET from a domain with a long neck)**.** *The MFPT of Brownian motion from a composite domain Ω with reflecting boundary to an absorbing boundary at the end of a narrow cylindrical neck of length L is given by*

$$\bar{\tau}_{\boldsymbol{x}\to\partial\Omega_a} = \bar{\tau}_{\boldsymbol{x}\to\partial\Omega_i} + \frac{L^2}{2D} + \frac{|\Omega_1|L}{|\partial\Omega_a|D}. \tag{6.5}$$

Proof. Consider the domain Ω in figure 20. Lemma 6.1 indicates how to sum the MFPTs. To calculate $\bar{\tau}_{\partial\Omega_i\to\partial\Omega_a}$ and the absorption flux at the interface the boundary value problem

$$\Delta v(\boldsymbol{x}) = -\frac{1}{D} \quad \text{for } \boldsymbol{x} \in \Omega \tag{6.6}$$

$$v(\boldsymbol{x}) = 0 \quad \text{for } \boldsymbol{x} \in \partial\Omega_a \tag{6.7}$$

$$\frac{\partial v(\boldsymbol{x})}{\partial n(\boldsymbol{x})} = 0 \quad \text{for } \boldsymbol{x} \in \partial\Omega_r \tag{6.8}$$

has to be solved in the narrow neck Ω_2. The solution can be approximated by that of the one-dimensional boundary value problem

$$Du_{zz} = -1 \quad \text{for } 0 < z < L, \quad u(0) = 0, \quad u(L) = u_H,$$

where the value at the interface $u(L) = u_H$ is yet unknown. The solution is given by

$$u(z) = -\frac{z^2}{2D} + Bz, \tag{6.9}$$

so that

$$u(L) = u_H = -\frac{L^2}{2D} + b.l., \tag{6.10}$$

where *b.l.* is a boundary layer term. Equation (6.10) relates the unknown constants B and u_H. The constant B is found by multiplying equation (6.6) by the Neumann function $N(\boldsymbol{x}, \boldsymbol{y})$, integrating over Ω_1, applying Green's formula, and using the boundary conditions (6.7) and (6.8). Specifically, we obtain for all $\boldsymbol{y} \in \partial\Omega_i$

$$v(\boldsymbol{y}) = -\frac{1}{D}\int_{\Omega_1} N(\boldsymbol{x}, \boldsymbol{y})\,\mathrm{d}\boldsymbol{x} - \int_{\partial\Omega_i} N(\boldsymbol{x}, \boldsymbol{y})\frac{\partial v(\boldsymbol{x})}{\partial n}\,\mathrm{d}S_x + \frac{1}{|\Omega_1|}\int_{\Omega_1} v(\boldsymbol{x})\,\mathrm{d}\boldsymbol{x}. \tag{6.11}$$

Approximating, as we may, $v(\boldsymbol{y}) \approx u(L)$ and using (6.10) gives

$$-\frac{L^2}{2D} + b.l. = -\frac{1}{D}\int_{\Omega_1} N(\boldsymbol{x}, \boldsymbol{y})\,\mathrm{d}\boldsymbol{x} - \int_{\partial\Omega_i} N(\boldsymbol{x}, \boldsymbol{y})\frac{\partial v(\boldsymbol{x})}{\partial n}\,\mathrm{d}S_x + \frac{1}{|\Omega_1|}\int_{\Omega_1} v(\boldsymbol{x})\,\mathrm{d}\boldsymbol{x}. \tag{6.12}$$

Because $v(\boldsymbol{x})$ is the solution of the boundary value problem (6.6)–(6.8) in the entire domain $\Omega = \Omega_1 \bigcup \Omega_2$, the meaning of (6.12) is the connecting rule (6.4), where

$$\bar{\tau}_{\boldsymbol{x}\to\partial\Omega_a} = \frac{1}{|\Omega_1|}\int_{\Omega_1} v(\boldsymbol{x})\,\mathrm{d}\boldsymbol{x} \tag{6.13}$$

$$\bar{\tau}_{\partial\Omega_i\to\partial\Omega_a} = u(L) \tag{6.14}$$

$$\bar{\tau}_{\boldsymbol{x}\to\partial\Omega_i} = -\frac{1}{D}\int_{\Omega} N(\boldsymbol{x},\boldsymbol{y})\,\mathrm{d}\boldsymbol{x} - \int_{\partial\Omega_i} N(\boldsymbol{x},\boldsymbol{y})\frac{\partial v(\boldsymbol{x})}{\partial n}\,\mathrm{d}S_{\boldsymbol{x}}. \tag{6.15}$$

Equation (6.13) gives the MFPT, averaged over Ω_1. The averaging is a valid approximation, because the MFPT to $\partial\Omega_i$ is constant to begin with (except in a negligible boundary layer). Equation (6.14) is the MFPT from the interface to the absorbing end $\partial\Omega_a$ of the strip, and (6.15) follows from the identity (Singer *et al* 2006c, Schuss 2013, Holcman and Schuss 2014)

$$0 = \frac{1}{D}\int_{\Omega} N(\boldsymbol{x},\boldsymbol{\xi})\,\mathrm{d}\boldsymbol{x} + \int_{\partial\Omega_a} N(\boldsymbol{x},\boldsymbol{\xi})g(\boldsymbol{x})\,\mathrm{d}S_{\boldsymbol{x}} + C_{\varepsilon}, \tag{6.16}$$

for all $\boldsymbol{\xi}\in\partial\Omega_a$. Matching the solutions in Ω_1 and Ω_2 continuously across $\partial\Omega_i$, the total flux on $\partial\Omega_i$ is obtained as

$$J = D\int_{\partial\Omega_i}\frac{\partial v(\boldsymbol{x})}{\partial \nu}\,\mathrm{d}S_{\boldsymbol{x}} = -\left(|\Omega_1| + |\Omega_2|\right). \tag{6.17}$$

Noting that $\partial v(\boldsymbol{x})/\partial n = -u'(0) = -B$, equations (6.1) and (6.17) give that

$$B = -\begin{cases} \dfrac{|\Omega_1|}{aD} + \dfrac{L}{D} & \text{for a line segment} \\ \dfrac{|\Omega_1|}{2\pi aD} + \dfrac{L}{D} & \text{for a circle} \\ \dfrac{|\Omega_1|}{\pi a^2 D} + \dfrac{L}{D} & \text{for a circular disk.} \end{cases} \tag{6.18}$$

Finally, equations (6.4)–(6.18) give (6.5). The NET $\bar{\tau}_{\boldsymbol{x}\to\partial\Omega_i}$ for the various domains is given in Holcman and Schuss (2014). □

Expression (6.5) for the NET from a two-dimensional domain with a bottleneck in the form of one-dimensional neck, such as a dendritic spine (figure 20 (left)), can be phrased as follows. Consider a domain Ω with head Ω_1 and a narrow cylindrical neck Ω_2 of length L and radius a. The radius of curvature at the bottleneck in a smooth connecting funnel is R_c. The following classification of the NET from a dendritic spine holds (figure 21),

$$\bar{\tau}_{\boldsymbol{x}\to\partial\Omega_a} = \begin{cases} \dfrac{|\Omega_1|}{\pi D}\ln\dfrac{|\partial\Omega_1|}{a} + \dfrac{O(1)}{D} + \dfrac{L^2}{2D} + \dfrac{|\Omega_1|L}{aD} \\ \text{planar spine connected to the neck at a right angle} \\ \dfrac{\pi|\Omega_1|}{D}\sqrt{\dfrac{R_c}{a}}\,(1+o(1)) + \dfrac{L^2}{2D} + \dfrac{|\Omega_1|L}{2\pi aD} \\ \text{planar spine with a smooth connecting funnel} \\ \dfrac{|\Omega_1|}{2\pi D}\log\dfrac{\sin\frac{\theta}{2}}{\sin\frac{\delta}{2}} + \dfrac{L^2}{2D} + \dfrac{|\Omega_1|L}{2\pi aD} \\ \text{spherical spine connected to the neck at a right angle} \\ \dfrac{|\Omega_1|}{2D}\dfrac{\left(\frac{\varepsilon}{\ell}\right)^{-\alpha/1+\alpha}2^{\alpha/1+\alpha}}{(1+\alpha)\sin\frac{\pi}{1+\alpha}} + \dfrac{L^2}{2D} + \dfrac{|\Omega_1|L}{2\pi aD} \\ \text{spherical spine with a smooth connecting funnel,} \end{cases} \tag{6.19}$$

where R is the radius of the sphere, $a = R\sin\delta/2$, and θ is the initial elevation angle on the sphere. If $|\Omega_1| \gg aL$ and $L \gg a$, the last term in (6.19) is dominant, which is the manifestation of the many returns of Brownian motion from the neck to the head prior to absorption at $\partial\Omega_a$ (see an estimate in Biess *et al* 2007). Formula (6.19) is used to estimate the residence time of receptors on the surface of a dendritic spine. A generalization to three dimensions is given in Holcman and Schuss (2012).

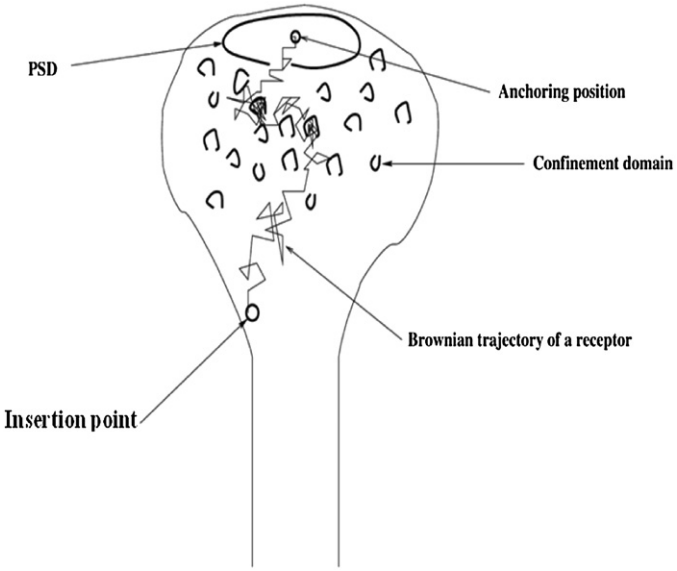

Figure 21. Receptor movement on the neuronal membrane.

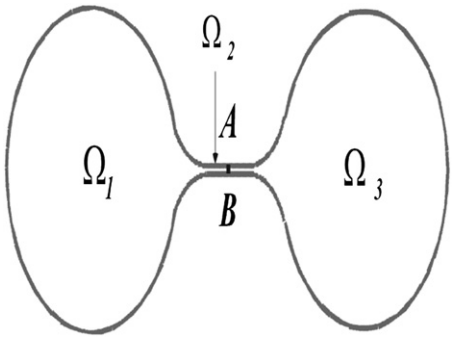

Figure 22. A dumbbell-shaped domain consists of two large compartments Ω_1 and Ω_3 connected by a narrow neck Ω_2. The bottleneck is the interval $\boldsymbol{AB}$.

6.1. Transition rate and the principal eigenvalue in composite domains

Consider, for simplicity, the sojourn time of Brownian motion in a compartment interconnected by a narrow neck to another compartment in a composite domain, as shown in figure 22. The sojourn time is the MFPT from that compartment to another one. In the limit of shrinking neck, the sojourn time is to leading order independent of the initial point of the escaping trajectory and equals twice the MFPT from the compartment to the narrowest passage in the bottleneck (e.g., the interval $\boldsymbol{AB}$ in figure 22). Indeed, the reciprocal of this MFPT is to leading order the rate at which trajectories reach the bottleneck from the first compartment, so the reciprocal of the MFPT is the lowest eigenvalue of the mixed Neumann–Dirichlet boundary value problem in the first compartment with Dirichlet conditions on the cross section of the neck.

There is a spectral gap of order one from the smallest eigenvalue to the next one. Thus, it follows that long transition times of Brownian trajectories between compartments connected by

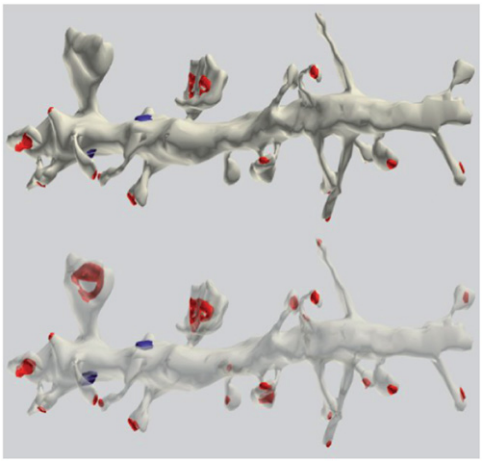

Figure 23. Three-dimensional EM reconstruction of two hippocampal dendrites with spines. The post-synaptic domain of excitatory synapses are marked red and of inhibitory synapses *m* blue. The dendritic spine geometry is approximated as the composite domain shown in figure 20 (left).

bottlenecks are exponentially distributed and therefore the leading eigenvalues of Neumann's problem for the Laplace equation in a domain that consists of compartments interconnected by narrow necks are to leading order the eigenvalues of a Markov chain with transition rates that are the reciprocals of the MFPTs through the narrow necks, as is the case for diffusion in a potential landscape with several deep wells (high barriers) (Schuss 2010b). The evaluation of the leading eigenvalues of the Neumann problem for the Laplace equation in domains with bottlenecks reduces to the computation of the leading order eigenvalues for the mixed Neumann–Dirichlet boundary value problem for the Laplace equation in domains with reflecting (Neumann) boundary, except for a small absorbing (Dirichlet) window at the end of a funnel.

6.2. The principal eigenvalue in a domain with a head and narrow neck

The composite domain Ω in figure 20 (left) consists of a head Ω_1 connected by a funnel to a narrow cylindrical neck Ω_2. The boundary of the domain is reflecting (Neumann) and only the far end of the cylinder $\partial\Omega_a$ is absorbing (Dirichlet). The left half of the dumbbell-shaped domain shown in figure 22 is a composite domain of this type if the interval $\boldsymbol{AB}$ is an absorbing boundary. In the three-dimensional case the Dirichlet boundary $\partial\Omega_a$ is a small absorbing disk at the end of the cylinder. The domain Ω_1 is the one shown in figure 24 and it is connected to the cylinder at an interface $\partial\Omega_i$, which in this case is the interval AB in figure 24. Using (6.5) and the fact that the principal eigenvalue of the mixed two- and three-dimensional Neumann–Dirichlet problems in domains with small Dirichlet and large Neumann parts of a smooth boundary is asymptotically the reciprocal of the MFPT, we find that the principal eigenvalue λ_1 in a domain with a single bottleneck is given by

$$\lambda_1 \sim \frac{1}{\bar{\tau}_{\boldsymbol{x}\to\partial\Omega_i} + \frac{L^2}{2D} + \frac{|\Omega_1|L}{|\partial\Omega_a|D}}, \tag{6.20}$$

where $\bar{\tau}_{\boldsymbol{x}\to\partial\Omega_i}$ is any one of the MFPTs given in (6.18), depending on the geometry of Ω_1.

If a composite domain consists of a single head and N well-separated bottlenecks of different radii and neck lengths, then the reciprocal of the MFPT is the sum of the reciprocals

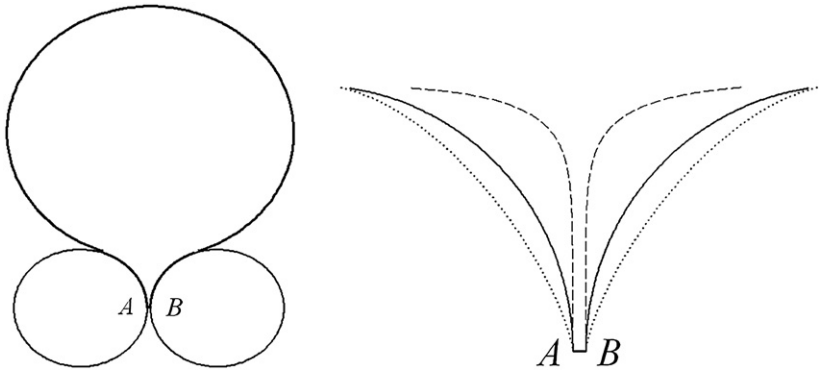

Figure 24. Cusp geometry. Left: the planar (dimensional) domain Ω' is bounded by a large circular arc connected smoothly to a funnel formed by moving two tangent circular arcs of radius $R_c\ \varepsilon$ apart (i.e., $\overline{AB} = \varepsilon$). Right: blowup of the cusp region. The solid, dashed, and dotted necks correspond to different curvatures of the neck.

of the NETs from a domain with a single bottleneck (Schuss 2013, Holcman and Schuss 2014). That is, the principal eigenvalue λ_P is given by

$$\lambda_P \sim \sum_{j=1}^{N} \lambda_j. \tag{6.21}$$

This can be interpreted as the fact that the total efflux is the sum of N independent effluxes through the bottlenecks.

6.3. The principal eigenvalue and coarse-grained diffusion in a dumbbell

A dumbbell-shaped domain Ω consists of two- or three-dimensional compartments Ω_1 and Ω_3 and a connecting neck Ω_2 that is effectively one-dimensional, as shown in figure 22. The stochastic separatrix (SS) in Ω is the locus of initial points for Brownian trajectories that are equally likely to reach Ω_1 before Ω_3 as they are to reach Ω_3 before Ω_1 (Ryter 1987a, 1987b, Schuss 2010a, 2013). In figure 22 the SS is the interval $\boldsymbol{AB}$. Consider the eigenvalue problem for the Laplace equation in Ω with Neumann boundary conditions.

Theorem 6.3 (The principal eigenvalue in a dumbbell)**.** *The smallest positive eigenvalue* λ *of the Neumann problem for the Laplace equation in the dumbbell is to leading order that of the two-state Markov process,*

$$\lambda = -(\lambda_{\mathrm{I}\to\mathrm{II}} + \lambda_{\mathrm{II}\to\mathrm{I}}),$$

where the transition rates from I to II and from II to I are, respectively,

$$\lambda_{\mathrm{I}\to\mathrm{II}} = \frac{1}{2\bar{\tau}_{\Omega_1\to SS}}, \quad \lambda_{\mathrm{II}\to\mathrm{I}} = \frac{1}{2\bar{\tau}_{\Omega_3\to SS}}. \tag{6.22}$$

Proof. Assuming, as we may, that the SS is the cross section of the neck at its center, the mean time to traverse the neck from Ω_1 to Ω_3 is asymptotically twice the MFPT $\bar{\tau}_{\boldsymbol{x}\to SS}$ from $\boldsymbol{x} \in \Omega_1$ to the SS (see Schuss 2010a). This MFPT is to leading order independent of $\boldsymbol{x} \in \Omega_1$ and can be denoted $\bar{\tau}_{\Omega_1\to SS}$. Note that when the neck is narrow the mean residence time of a Brownian

trajectory in Ω_1 or in Ω_3 is much longer than that in Ω_2. Also note that the first passage time $\tau_{\boldsymbol{x}\to SS}$ for $\boldsymbol{x}\in\Omega_1$ is exponentially distributed for long times and so is $\tau_{\boldsymbol{x}\to SS}$ for $\boldsymbol{x}\in\Omega_3$ (Schuss 2010b). Therefore the Brownian motion in Ω can be coarse-grained into a two-state Markov process (a telegraph process), which is in State I when the Brownian trajectory is in Ω_1 and is in State II when it is in Ω_3. The state Ω_2 and the residence time there can be neglected relative to those in Ω_1 and Ω_3. The transition rates from I to II and from II to I, given in (6.22), can be found from (6.20), with L half the length of the neck and $SS=\partial\Omega_a$. The radii of curvature $R_{c,1}$ and $R_{c,3}$ at the two funnels may be different, and the domain is either Ω_1 or Ω_3, as the case may be.

The asymmetric Markovian random telegraph process jumps between two states, I and II, at independent exponentially distributed waiting times with rates $\lambda_{\mathrm{I}\to\mathrm{II}}$ and $\lambda_{\mathrm{II}\to\mathrm{I}}$, respectively. The transition probability distribution function satisfies the linear differential equations[6] (Schuss 2010b)

$$\begin{aligned}\frac{\mathrm{d}P\{I,t\,|\,x,t_0\}}{\mathrm{d}t}&=-\lambda_{\mathrm{I}\to\mathrm{II}}P\{\mathrm{I},t\,|\,x,t_0\}+\lambda_{\mathrm{II}\to\mathrm{I}}P\{\mathrm{II},t\,|\,x,t_0\}\\ \frac{\mathrm{d}P\{\mathrm{II},t\,|\,x,t_0\}}{\mathrm{d}t}&=\lambda_{\mathrm{I}\to\mathrm{II}}P\{\mathrm{I},t\,|\,x,t_0\}-\lambda_{\mathrm{II}\to\mathrm{I}}P\{\mathrm{II},t\,|\,x,t_0\},\end{aligned}\tag{6.23}$$

which can be written in the obvious matrix notation as $\dot{\boldsymbol{p}}=\boldsymbol{A}\boldsymbol{p}$ with

$$\boldsymbol{A}=\begin{pmatrix}-\lambda_{\mathrm{I}\to\mathrm{II}} & \lambda_{\mathrm{II}\to\mathrm{I}}\\ \lambda_{\mathrm{I}\to\mathrm{II}} & -\lambda_{\mathrm{II}\to\mathrm{I}}\end{pmatrix}.$$

The eigenvalues of $\boldsymbol{A}$ are 0 with the normalized eigenvector $(\frac{1}{2},\frac{1}{2})^T$, and $-(\lambda_{\mathrm{I}\to\mathrm{II}}+\lambda_{\mathrm{II}\to\mathrm{I}})$ with the eigenvector $(1,-1)^T$. It follows that the nonzero eigenvalue of the system (6.23) is $\lambda=\lambda_{\mathrm{I}\to\mathrm{II}}+\lambda_{\mathrm{II}\to\mathrm{I}}$. Hence the theorem follows. □

For example, if the solid dumbbell consists of two general heads connected smoothly to the neck by funnels, the two rates are given by (Schuss 2013, Holcman and Schuss 2014)

$$\frac{1}{\lambda_{\mathrm{I}\rightleftarrows\mathrm{II}}}=\sqrt{2}\left[\left(\frac{R_{c,1/3}}{a}\right)^{3/2}\frac{|\Omega_{1/3}|}{R_{c,1/3}D}\right][1+o(1)]+\frac{L^2}{4D}+\frac{|\Omega_{1/3}|L}{\pi a^2 D}.\tag{6.24}$$

Consider, for example, the Neumann problem for the Laplace equation in a domain that consists of any number of heads interconnected by narrow necks. The Brownian motion can be coarse-grained into a Markovian random walk that jumps between the connected domains at exponentially distributed times with rates determined by the first passage times and exit probabilities, as described in section 6.2. This random walk can in turn be approximated by an effective coarse-grained anisotropic diffusion, as done, for example, for atomic migration in crystals (Schuss 1980, chapter 8, section 2), for effective diffusion on a surface with obstacles (see section 3.1 and (Holcman *et al* 2011)), and for a general diffusion on a potential landscape with deep wells (Hänggi *et al* 1990).

Some estimates of the asymptotic behavior of the leading eigenvalue in dumbbell-shaped domains are given in Arrieta (1995), Ward and Stafford (1999), Jimbo and Kosugi (2009), Dagdug *et al* (2003), and references therein.

6.4. Diffusional transfer of genetic material during cell division

During cell division, daughter and mother cells remain connected by a neck that grows narrow until it breaks off. The two connected cells have the shape of an asymmetric dumbbell. During this division process, some of the genetic (mRNA and TFs) material is delivered from the

[6] see http://en.wikipedia.org/wiki/Telegraph_process.

mother to the daughter cell. It remains unclear how this genetic material is selected. A recent report (Gehlen *et al* 2011) proposes that diffusion through the connecting neck is the main determinant of the delivery rate and of the selection of fast diffusing particles during the transient regime, before steady state is reached. The effect of asymmetry in the curvature of the connecting neck in the dumbbell can be analyzed in the limit of a narrow neck. The transition rates between the two cells can differ by orders of magnitude as the geometry changes. This can be used to re-interpret the findings reported experimentally in Gehlen *et al* (2011).

7. Summary and discussion

This review presents recent progress in stochastic modeling in cellular biology and in coarse-graining molecular-level models of Brownian motion in biological cells or on their membranes into the cellular scale, where cell function can be discerned. The key factor in this coarse-graining is the time scale of passage time through narrow necks. The passage through small openings or narrow passages emerges as the main flux-controlling machinery on the cellular level. The coarse-grained models are used to analyze and simulate models of subcellular processes, to quantify their biological functions, and are the basis for data analysis. The analytical details of the asymptotic expansion of the narrow escape theory (NET) are reviewed in Holcman and Schuss (2014) and Schuss (2013).

The models and analysis presented here can be extended in several directions. The theory of threshold in chemical reactions can be used to quantify checkpoint processes in biology, such as the induction of plasticity (Dao Duc and Holcman 2010), the decision to start spindle separation during cell replication (Dao Duc and Holcman 2012) or any other decision process that occurs when a certain number of molecules are activated. The model of virus trafficking can be extended to enveloped viruses. Other steps of viral infection should be further modeled, such as the insertion of the genetic material to a DNA site, the synthesis part, the formation of the capsid and budding. Another direction is the search for a promoter site in the cell nucleus. Indeed, a key feature in the search by a TF is the local structure of the DNA conformation and chromatin near the specific binding site. So far no modeling approach has been proposed that integrates the DNA organization into the algorithm for estimating of the mean time to find the DNA promoter site. It would be interesting to combine polymer dynamics in microdomains with the NET. The methodology presented here can be applied to the modeling of synaptic transmission and extended to include various molecular feedbacks implied in modulating the probability of vesicular release.

Acknowledgment

This research is supported by an ERC-starting-Grant.

References

Abe A, Miyanohara A and Friedmann T 1998 Enhanced gene transfer with fusogenic liposomes containing vesicular stomatitis virus G glycoprotein *J. Virol.* **72** 6159–63

Alberts B, Bray D, Lewis J, Raff M, Roberts K and Watson J D 1994 *Molecular Biology of the Cell* (New York: Garland)

Amitai A and Holcman D 2013 Polymer model with long-range interactions: analysis and applications to the chromatin structure *Phys. Rev.* E **88** 052604

Amitai A, Kantor Y and Kardar M 2010 First-passage distributions in a collective model of anomalous diffusion with tunable exponent *Phys. Rev.* E **81** 011107

Amoruso C, Lagache T and Holcman D 2011 Modeling the early steps of cytoplasmic trafficking in viral infection and gene delivery *SIAM. J. Appl. Math.* **71** 2334–58
Arrieta J M 1995 Rates of eigenvalues on a dumbbell domain. Simple eigenvalue case *Trans. Am. Math. Soc.* **347** 3503–31
Barkai E, Garini Y and Metzler R 2012 Strange kinetics of single molecules in living cells *Phys. Today* **65** 29
Bénichou O, Coppey M, Moreau M, Suet P H and Voituriez R 2005 A stochastic model for intermittent search strategies *J. Phys.: Condens. Matter* **17** 4275–86
Berezhkovskii A M and Barzykin A V 2012 Search for a small hole in a cavity wall by intermittent bulk and surface diffusion *J. Chem. Phys.* **136** 054115
Biess A, Korkotian E and Holcman D 2007 Diffusion in a dendritic spine: the role of geometry *Phys. Rev.* E **76** 021922
Bloodgood B L and Sabatini B L 2005 Neuronal activity regulates diffusion across the neck of dendritic spines *Science* **310** 866–9
Borgdorff A J and Choquet D 2002 Regulation of AMPA receptor lateral movements *Nature* **417** 649–53
Bourne J N and Harris K M 2008 Balancing structure and function at hippocampal dendritic spines *Annu. Rev. Neurosci.* **31** 47–67
Bouzigues C, Morel M, Triller A and Dahan M 2007 Asymmetric redistribution of GABA receptors during GABA gradient sensing by nerve growth cones analyzed by single quantum dot imaging *Proc. Natl Acad. Sci. USA* **104** 11251–6
Bouzigues C, Holcman D and Dahan M 2010 A mechanism for the polarity formation of chemoreceptors at the growth cone membrane for gradient amplification during directional sensing *PLoS One* **5** e9243
Brandenburg B and Zhuang X 2007 Virus trafficking—learning from single-virus tracking *Nature Rev. Microbiol.* **5** 197–208
Bredt D S and Nicoll R A 2003 AMPA receptor trafficking at excitatory synapses *Neuron* **40** 361–79
Bressloff P C and Earnshaw B A 2009 A dynamical corral model of protein trafficking in spines *Biophys. J.* **96** 1786–802
Bressloff P C and Newby J M 2013 Stochastic models of intracellular transport *Rev. Mod. Phys.* **85** 135
Burger M, Eisenberg R S and Engl H W 2007 Inverse problems related to ion channel selectivity *SIAM J. Appl. Math.* **67** 960–89
Chen D P, Lear J and Eisenberg R S 1997 Permeation through an open channel: Poisson–Nernst–Planck theory of a synthetic ionic channel *Biophys. J.* **72** 97–116
Choquet D 2010 Fast AMPAR trafficking for a high-frequency synaptic transmission *Eur. J. Neurosci.* **32** 250–60
Choquet D and Borgdorff A J 2002 Regulation of AMPA receptor lateral movements *Nature* **417** 649–53
Coppey M, Bénichou O, Voituriez R and Moreau M 2004 Kinetics of target site localization of a protein on DNA: a stochastic approach *Biophys. J.* **87** 1640–9
Cowan W M, Südhof T C and Stevens C F (ed) 2003 *Synapses* (Baltimore, MD: Johns Hopkins University Press)
Dagdug L, Berezhkovskii A M, Shvartsman S Y and Weiss G H 2003 Equilibration in two chambers connected by a capillary *J. Chem. Phys.* **119** 12473–8
Dao Duc K and Holcman D 2010 Threshold activation for stochastic chemical reactions in microdomains *Phys. Rev.* E **81** 041107
Dao Duc K and Holcman D 2012 Using default constraints of the spindle assembly checkpoints to estimate the associate chemical rates *BMC Biophys.* **5** 1
Dauty E and Verkman A S 2005 Actin cytoskeleton as the principal determinant of size-dependent DNA mobility in cytoplasm: a new barrier for non-viral gene delivery *J. Biol. Chem.* **280** 7823–8
Doering C 2000 Effect of boundary condition fluctuations on Smoluchowski reaction rates *Stochastic Processes in Physics, Chemistry, and Biology Lecture Notes in Physics* vol 557 (New York: Springer) pp 316–26
Edidin M, Kuo S C and Sheetz M P 1991 Lateral movements of membrane glycoproteins restricted by dynamic cytoplasmic barriers *Science* **254** 1379–82
Eisinger J, Flores J and Petersen W P 1986 A milling crowd model for local and long-range obstructed lateral diffusion. Mobility of excimeric probes in the membrane of intact erythrocytes *Biophys. J.* **49** 987–1001
Elf J, Li G and Xie X 2007 Probing transcription factor dynamics at the single-molecule level in a living cell *Science* **316** 1191

Fabrikant V I 1989 *Applications of Potential Theory in Mechanics* (Dodrecht: Kluwer)
Fabrikant V I 1991 *Mixed Boundary Value Problems of Potential Theory and Their Applications in Engineering* (Dodrecht: Kluwer)
Farr G A, Zhang L G and Tattersall P 2005 Parvoviral virions deploy a capsid-tethered lipolytic enzyme to breach the endosomal membrane during cell entry *Proc. Natl Acad. Sci. USA* **102** 17148–53
Freche D, Pannasch U, Rouach N and Holcman D 2011 Synapse geometry and receptor dynamics modulate synaptic strength *PLoS One* **6** e25122
Furini S, Domene C and Cavalcanti S 2010 Insights into the sliding movement of the lac repressor nonspecifically bound to DNA *J. Phys. Chem.* B **114** 2238–45
Gebhardt C and Cull-Candy S G 2006 Influence of agonist concentration on AMPA and kainate channels in CA1 pyramidal cells in rat hippocampal slices *J. Physiol.* **573** 371–94
Gehlen L R, Nagai S, Shimada K, Meister P, Taddei A and Gasser S M 2011 Nuclear geometry and rapid mitosis ensure asymmetric episome segregation in yeast *Curr. Biol.* **21** 25–33
Gillespie D T 1976 A general method for numerically simulating the stochastic time evolution of coupled chemical reactions *J. Comput. Phys.* **22** 403–34
Greber U F and Way M 2006 A superhighway to virus infection *Cell* **124** 741–54
Grigoriev I V, Makhnovskii Y A, Berezhkovskii A M and Zitserman V Y 2002 Kinetics of escape through a small hole *J. Chem. Phys.* **116** 9574–7
Hänggi P, Talkner P and Borkovec M 1990 *Rev. Mod. Phys.* **62** 251–341
Harris K M and Stevens J K 1988 Dendritic spines of rat cerebellar purkinje cells: serial electron microscopy with reference to their biophysical characteristics *J. Neurosci.* **12** 4455–69
Hille B 2001 *Ionic Channels of Excitable Membranes* 3rd edn (Sunderland, MA: Sinauer Associates Inc.)
Hoefling F and Franosch T 2013 *Rep. Prog. Phys.* **76** 046602
Holcman D, Hoze N and Schuss Z 2011 Narrow escape through a funnel and effective diffusion on a crowded membrane *Phys. Rev.* E **84** 021906
Holcman D, Korkotian E and Segal M 2005a Calcium dynamics in dendritic spines, modeling and experiments *Cell Calcium* **37** 467–75
Holcman D 2007 Modeling viral and DNA trafficking in the cytoplasm of a cell *J. Stat. Phys.* **127** 471–94
Holcman D and Kupka I 2010 Some questions in computational cellular biology *J. Fixed Point Theory Appl.* **7** 67–83
Holcman D, Marchewka A and Schuss Z 2005b The survival probability of diffusion with trapping in cellular biology *Phys. Rev.* E **72** 031910
Holcman D and Schuss Z 2004 Escape through a small opening: receptor trafficking in a synaptic membrane *J. Stat. Phys.* **117** 191–230
Holcman D and Schuss Z 2005 Stochastic chemical reactions in microdomains *J. Chem. Phys.* **122** 114710
Holcman D and Schuss Z 2011 Diffusion laws in dendritic spines *J. Math. Neurosci.* **1** 10
Holcman D and Schuss Z 2012 Brownian motion in dire straits *SIAM. J. Multiscale Modeling Simul.* **10** 1204–31
Holcman D and Schuss Z 2014 The narrow escape problem *SIAM Rev.* at press
Holcman D, Schuss Z and Korkotian E 2004 Calcium dynamics in dendritic spines and spine motility *Biophys. J.* **87** 81–91
Holcman D and Triller A 2006 Modeling synaptic dynamics and receptor trafficking *Biophys. J.* **91** 2405–15
Hotulainen P and Hoogenraad C C 2010 Actin in dendritic spines: connecting dynamics to function *J. Cell Biol.* **189** 619–29
Hoze N, Nair D, Hosy E, Sieben C, Manley S, Herrmann A, Sibarita J B, Choquet D and Holcman D 2012 Heterogeneity of AMPA receptor trafficking and molecular interactions revealed by superresolution analysis of live cell imaging *Proc. Natl Acad. Sci. USA* **109** 17052–7
Huang Q, Opitz R, Knapp E W and Herrmann A 2002 Protonation and stability of the globular domain of influenza virus hemagglutinin *Biophys. J.* **82** 1050–8
Jeon J H, Tejedor V, Burov S, Barkai E, Selhuber-Unkel C, Berg-Sorensen K, Oddershede L and Metzler R 2011 *In vivo* anomalous diffusion and weak ergodicity breaking of lipid granules *Phys. Rev. Lett.* **106** 048103
Jimbo S and Kosugi S 2009 Spectra of domains with partial degeneration *J. Math. Sci. Univ. Tokyo* **16** 269–414

Jonas P, Major G and Sakmann B 1993 Quantal components of unitary EPSCs at the mossy fibre synapse on CA3 pyramidal cells of a rat hippocampus *J. Physiol.* **472** 615–63

Kandel E R, Schwartz J H and Jessell T M 2000 *Principles of Neural Science* 4th edn (New York: McGraw-Hill)

Kim S H, Wang W and Kim K K 2002 Dynamic and clustering model of bacterial chemotaxis receptors: structural basis for signaling and high sensitivity *Proc. Natl Acad. Sci. USA* **99** 11611–5

Knessl C, Mangel M, Matkowsky B J and Schuss Z 1984a Solution of Kramers–Moyal equations for problems in chemical physics *J. Chem. Phys.* **81** 1285–93

Knessl C, Matkowsky B J, Schuss Z and Tier C 1984b An asymptotic theory of large deviations for Markov jump processes *SIAM J. Appl. Math.* **45** 1006–102

Kolokolnikov T, Titcombe M and Ward M J 2005 Optimizing the fundamental Neumann eigenvalue for the Laplacian in a domain with small traps *Eur. J. Appl. Math.* **16** 161–200

Korkotian E, Holcman D and Segal M 2004 Dynamic regulation of spine-dendrite coupling in cultured hippocampal neurons *Eur. J. Neurosci.* **20** 2649–63

Kusumi A, Nakada C, Ritchie K, Murase K, Suzuki K, Murakoshi H, Kasai R S, Kondo J and Fujiwara T 2005 Paradigm shift of the plasma membrane concept from the two-dimensional continuum fluid to the partitioned fluid: high-speed single-molecule tracking of membrane molecules *Annu. Rev. Biophys. Biomol. Struct.* **34** 351–78

Kusumi A, Sako Y and Yamamoto M 1993 Confined lateral diffusion of membrane receptors as studied by single particle tracking (nanovid microscopy). Effects of calcium-induced differentiation in cultured epithelial cells *Biophys. J.* **65** 2021–40

Lagache T, Danos O and Holcman D 2012 Modeling the step of endosomal escape during cell infection by a nonenveloped virus *Biophys. J.* **102** 980–9

Lagache T, Dauty E and Holcman D 2009a Physical principles and models describing intracellular virus particle dynamics *Curr. Opin. Microbiol.* **12** 439–45

Lagache T, Dauty E and Holcman D 2009b Quantitative analysis of virus and plasmid trafficking in cells *Phys. Rev.* E **79** 011921

Lagache T and Holcman D 2008a Effective motion of a virus trafficking inside a biological cell *SIAM. J. Appl. Math.* **68** 1146–67

Lagache T and Holcman D 2008b Quantifying intermittent transport in cell cytoplasm *Phys. Rev.* E **77** 030901

MacKinnon R 2003 Potassium channels and the atomic basis of selective ion conduction *Nobel Lecture 2003* www.nobelprize.org/nobel_prizes/chemistry/laureates/2003/mackinnon-lecture.html

Madison D V, Malenka R C and Nicoll R A 1991 Mechanisms underlying long-term potentiation of synaptic transmission *Annu. Rev. Neurosci.* **14** 379–397

Majewska A, Brown E, Ross J and Yuste R 2000 Mechanisms of calcium decay kinetics in hippocampal spines: role of spine calcium pumps and calcium diffusion through the spine neck in biochemical compartmentalization *J. Neurosci.* **20** 1722–34

Malherbe G and Holcman D 2010 The search for a DNA target in the nucleus *Phys. Lett.* A **374** 466–71

Malinow R and Malenka R C 2002 AMPA receptor trafficking and synaptic plasticity *Annu. Rev. Neurosci.* **25** 106–26

Matkowsky B J, Schuss Z, Knessl C, Tier C and Mangel M 1984 Asymptotic solution of the Kramers–Moyal equation and first-passage times for Markov jump processes *Phys. Rev.* A **29** 3359–69

Mattos T G, Meja-Monasterio C, Metzler R, Oshanin G and Schehr G 2012 Trajectory-to-trajectory fluctuations in first-passage phenomena in bounded domains *Phys. Rev.* E **86** 031143

Nadler B, Naeh T and Schuss Z 2002 The stationary arrival process of diffusing particles from a continuum to an absorbing boundary is Poissonian *SIAM J. Appl. Math.* **62** 433–47

Newpher T M and Ehlers M D 2009 Spine microdomains for postsynaptic signaling and plasticity *Trends Cell Biol.* **5** 218–27

Oshanin G, Tamm M and Vasilyev O 2010 Narrow-escape times for diffusion in microdomains with a particle-surface affinity: mean-field results *J. Chem. Phys.* **132** 235101

Popov I Yu 1992 Extension theory and localization of resonances for domains of trap type *Math. USSR Sb.* **71** 209–34

Rachakonda P S, Veit M, Korte T, Ludwig K, Böttcher C, Huang Q, Schmidt M F G and Herrmann A 2007 The relevance of salt bridges for the stability of the influenza virus hemagglutinin *FASEB J.* **21** 995–1002

Rayleigh J W S 1945 *The Theory of Sound* vol 2 2nd edn (New York: Dover)

Reingruber J, Abad E and Holcman D 2009 Narrow escape time to a structured target located at the boundary of a microdomian *J. Chem. Phys.* **130** 094909
Reingruber J and Holcman D 2009 The gated narrow escape time for molecular signaling *Phys. Rev. Lett.* **103** 148102
Reingruber J and Holcman D 2010 Narrow escape for a stochastically gated Brownian ligand *J. Phys.: Condens. Matter* **22** 065103
Reingruber J and Holcman D 2011a The narrow escape problem in a flat cylindrical microdomain, with application to diffusion in the synaptic cleft *Multiscale Modeling Simul.* **9** 793–816
Reingruber J and Holcman D 2011b Transcription factor search for a DNA promoter in a three-state model *Phys. Rev.* E **84** 020901
Renner M, Choquet D and Triller A 2009 Control of the postsynaptic membrane viscosity *J. Neurosci.* **29** 2926–637
Rosenmund C, Stern-Bach Y and Stevens C F 1998 The tetrameric structure of a glutamate receptor channel *Science* **280** 1596–9
Ryter D 1987a Noise-induced transitions in a double-well potential at low friction *J. Stat. Phys.* **49** 751–65
Ryter D 1987b On the eigenfunctions of the Fokker–Planck operator and of its adjoint *Physica* A **142** 103–21
Sakmann B and Neher E 2010 *Single-Channel Recording* (New York: Springer)
Saxton M J 1995 Single-particle tracking: effects of corrals *Biophys. J.* **69** 389–98
Saxton M J and Jacobson K 1997 Single-particle tracking: applications to membrane dynamics *Annu. Rev. Biophys. Biomol. Struct.* **26** 373–99
Schuss Z 1980 *Theory and Applications of Stochastic Differential Equations* (New York: Wiley)
Schuss Z 2010a Equilibrium and recrossings of the transition state: What can be learned from diffusion? *J. Phys. Chem.* C **114** 20320–34
Schuss Z 2010b *Theory and Applications of Stochastic Processes, and Analytical Approach Applied Mathematical Sciences* vol 170 (New York: Springer)
Schuss Z 2013 *Brownian Dynamics at Boundaries and Interfaces in Physics, Chemistry, and Biology (Applied Mathematical Sciences)* (New York: Springer)
Schuss Z, Singer A and Holcman D 2007 The narrow escape problem for diffusion in cellular microdomains *Proc. Natl Acad. Sci. USA* **104** 16098–103
Schuss Z and Spivak A 2005 On recovering the shape of a domain from the trace of the heat kernel *SIAM J. Appl. Math.* **66** 339–60
Segal M and Andersen P 2000 Dendritic spines shaped by synaptic activity *Curr. Opin. Neurobiol.* **10** 582–6
Seisenberger G, Ried M U, Endress T, Brüning H, Hallek M and Bräuchle 2001 Real-time single-molecule imaging of the infection pathway of an adeno-associated virus *Science* **294** 1929–32
Sheetz M P 1993 Glycoprotein motility and dynamic domains in fluid plasma membranes *Annu. Rev. Biophys. Biomol. Struct.* **22** 417–31
Shi S H, Hayashi Y, Petralia R S, Zaman S H, Wenthold R J, Svoboda K and Malinow R 1999 Rapid spine delivery and redistribution of AMPA receptors after synaptic NMDA receptor activation *Science* **284** 1811–6
Singer A, Schuss Z and Holcman D 2006a Narrow escape. Part II. The circular disk *J. Stat. Phys.* **122** 465–89
Singer A, Schuss Z and Holcman D 2006b Narrow escape: part III. Non-smooth domains and Riemann surfaces *J. Stat. Phys.* **122** 491–509
Singer A, Schuss Z and Holcman D 2008 Narrow escape and leakage of Brownian particles *Phys. Rev.* E **78** 051111
Singer A, Schuss Z, Holcman D and Eisenberg R S 2006c Narrow escape: part I *J. Stat. Phys.* **122** 437–63
Spacek J 2002 Synapse and dentric spine: three-dimensional view of effective tandem *Psychiatric* Suppl. 3 **6** 55–60
Sodeik B 2000 Mechanisms of viral transport in the cytoplasm *Trends Microbiol.* **8** 465–72
Suzuki K and Sheetz M P 2001 Binding of cross-linked glycosylphosphat-idylinositol-anchored proteins to discrete actin-associated sites and cholesterol-dependent domains *Biophys. J.* **81** 2181–9
Svoboda K, Tank D W and Denk W 1996 Direct measurement of coupling between dendritic spines and shafts *Science* **272** 716–9
Tabei S M, Burov S, Kim H Y, Kuznetsov A, Huynh T, Jureller J, Philipson L H, Dinner A R and Scherer N F 2013 Intracellular transport of insulin granules is a subordinated random walk *Proc. Natl Acad. Sci. USA* **110** 4911

Taflia A and Holcman D 2011 Estimating the synaptic current in a multiconductance AMPA receptor model *Biophys. J.* **101** 781–92

Tardin C, Cognet L, Bats C, Lounis B and Choquet D 2003 Direct imaging of lateral movements of AMPA receptors inside synapses *Embo J.* **22** 4656–65

Triller A and Choquet D 2003 The role of receptor diffusion in the organization of the postsynaptic membrane *Nature Rev. Neurosci.* **4** 1251–65

Tsaneva K, Burgo A, Galli T and Holcman D 2009 Quantifying neurite growth mediated by interactions between secretory vesicles, microtubules and actin networks *Biophys. J.* **96** 840–57

Tu Y and Kim J S 2008 A fusogenic segment of glycoprotein H from herpes simplex virus enhances transfection efficiency of cationic liposomes *J. Gene Med.* **10** 646–54

Verkman A S 2002 Solute and macromolecule diffusion in cellular aqueous compartments *Trends Biochem. Sci.* **27** 27–33

Von Hippel P and Berg O G 1989 Facilitated target location in biological systems *J. Biol. Chem.* **264** 675–8

Wang Y, Austin R and Cox E 2006 Single molecule measurements of repressor protein 1D diffusion on DNA *Phys. Rev. Lett.* **97** 048302

Ward M J and Keller J B 1993 Strong localized perturbations of eigenvalue problems *SIAM J. Appl. Math.* **53** 770–98

Ward M J and Stafford D 1999 Metastable dynamics and spatially inhomogeneous equilibria in dumbell-shaped domains *Stud. Appl. Math.* **103** 51–73

Whittaker G R, Kann M and Helenius A 2000 Viral entry into the nucleus *Annu. Rev. Cell Dev. Biol.* **16** 627–51

Zwanzig R 1990 Diffusion-controlled ligand binding to spheres covered by receptors: an effective medium treatment. *Proc. Natl Acad. Sci. USA* **87** 5856–7